Agricultural and Forest Meteorology 345 (2024) 109854

Contents lists available at ScienceDirect

Agricultural and Forest Meteorology

journal homepage: www.elsevier.com/locate/agrformet

Impacts of irrigation on a precipitation event during GRAINEX in the High Plains Aquifer Region

Daniel Whitesel [a,b], Rezaul Mahmood [a,b,*], Paul Flanagan [c], Eric Rappin [d], Udaysankar Nair [e], Roger A. Pielke Sr. [f,g], Michael Hayes [b]

[a] High Plains Regional Climate Center, School of Natural Resources, University of Nebraska-Lincoln, Lincoln, NE 68583, United States
[b] School of Natural Resources, University of Nebraska-Lincoln, Lincoln, NE 68583, United States
[c] U.S. Department of Agriculture-Agricultural Research Service, El Reno, OK 73036, United States
[d] Kentucky Climate Center, Western Kentucky University, Bowling Green, KY 42101, United States
[e] Department of Atmospheric Science, University of Alabama in Huntsville, Huntsville, AL 35806, United States
[f] Department of Atmospheric and Oceanic Sciences, University of Colorado-Boulder, Boulder, CO 80309, United States
[g] Cooperative Institute for Research in Environmental Sciences, University of Colorado-Boulder, Boulder, CO 80309, United States

ARTICLE INFO

Keywords:
Irrigation
GRAINEX
LULCC
Precipitation

ABSTRACT

Land use land cover change, including irrigation, impacts weather and climate. In this paper a precipitation event that occurred on the morning of 23 July 2018 during the Great Plains Irrigation Experiment (GRAINEX) is investigated. Six Weather and Research Forecasting (WRF) model-based experiments were conducted, which involved the increase or decrease of soil moisture by 5 % and up to 15 % over the irrigated croplands. These changes approximated soil moisture content in response to different levels of irrigation applications. An additional experiment, where irrigated land use was changed to grassland, was conducted to capture pre-irrigation land use and its impacts. It was found that regardless of strength of irrigation, precipitation decreased. In addition, the model did not produce precipitation over non-irrigated land use. When grassland replaced irrigated agriculture, increases in precipitation were estimated. With increased irrigation, latent heat flux increased compared to the control simulation and decreased when irrigation decreased. On the other hand, sensible heat flux was decreased compared to control when irrigation increased. The planetary boundary layer over irrigated land use was shallower than over non-irrigated land use while over grassland it was higher than irrigated but lower than non-irrigated land use. The changes in precipitation, the surface energy balance, and the planetary boundary layer served as a reminder of irrigation's complex effects on the atmosphere. Additional analysis of other precipitation events during GRAINEX would be helpful to better understand the effects of irrigation.

1. Introduction

Long-term biophysical and biogeochemical effects of land use land cover change (LULCC) have been well-documented (Pielke et al., 2011; Mahmood et al., 2014). For example, LULCC has been shown to affect the surface energy balance, moisture budget, and other land surface properties (Kueppers and Snyder, 2012; Xu et al., 2015; Pielke et al., 2016; Nauert and Ancell, 2019; Szilagyi and Franz, 2020). These changes can alter local and regional circulations, precipitation, and temperatures (Barnston and Schickedanz, 1984; Mahmood et al., 2004, 2006, 2013; Lobell and Bonfils, 2008; Cook et al., 2011; Sen Roy et al., 2011; Kang and Eltahir, 2019; Lawston et al., 2020; Rappin et al., 2021; Taylor et al., 2022).

Irrigated agriculture has been identified as an extensive form of LULCC (Nikiel and Eltahir, 2019). Irrigation introduces additional water, which in turn increases latent heat fluxes at the expense of sensible heat fluxes (Huber et al., 2014; Nikiel and Eltahir, 2019). This type of modification in energy partitioning has been shown to induce near surface cooling (Mahmood et al., 2013; Nikiel and Eltahir, 2019). Widespread irrigation has been adopted in the Great Plains to increase agricultural yield and due to the availability of groundwater from the Ogallala aquifer, also known as the High Plains Aquifer (HPA) (Evett

Submitted to: Agricultural and Forest Meteorology
* Corresponding author.
E-mail address: rmahmood2@unl.edu (R. Mahmood).

https://doi.org/10.1016/j.agrformet.2023.109854
Received 19 February 2023; Received in revised form 2 November 2023; Accepted 4 December 2023
Available online 13 December 2023

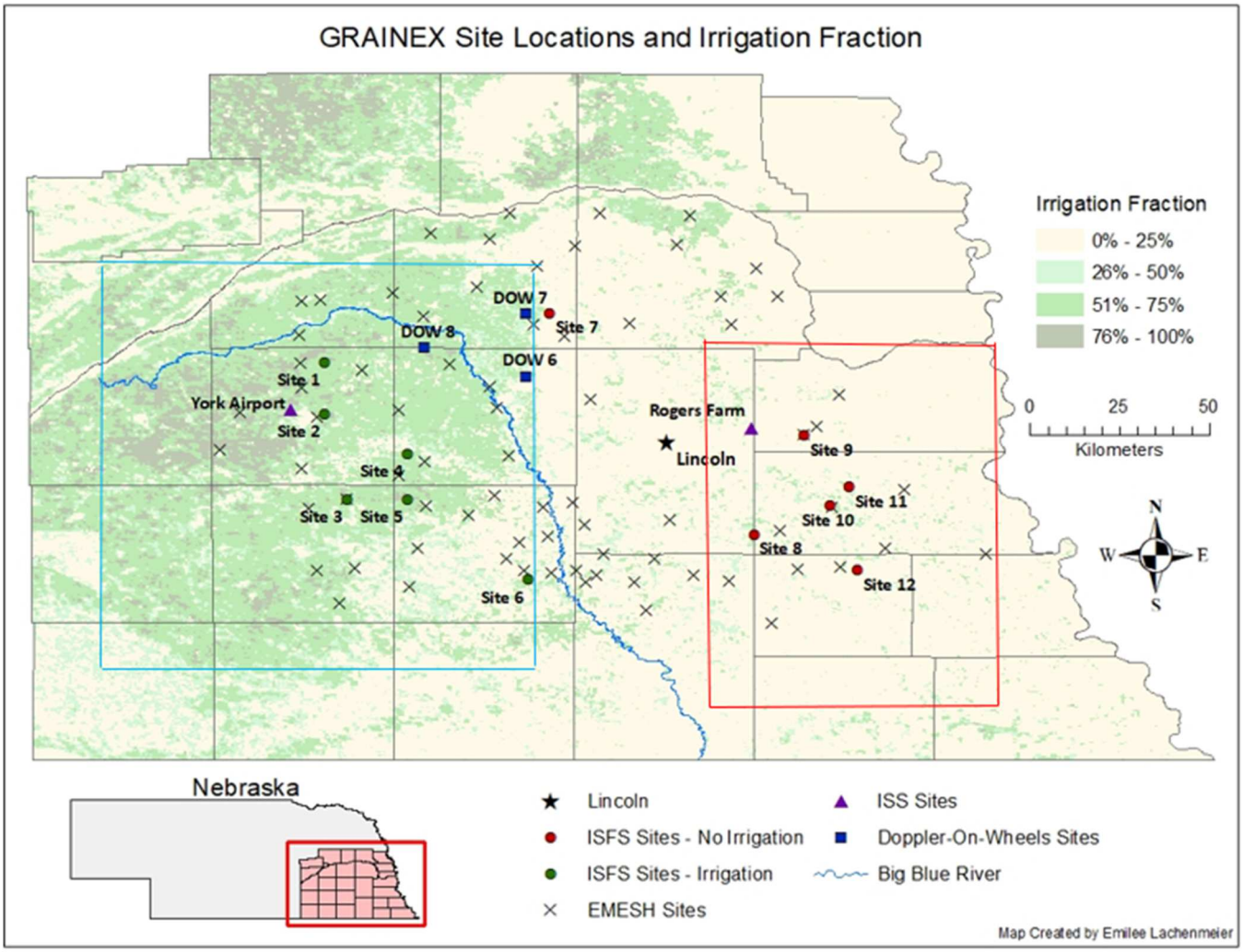

Fig. 1. The GRAINEX field campaign study area (Modified from Lachenmeier, 2020). ISFS is Integrated Surface Flux Site; ISS is Integrated Sounding System; DOW is Doppler on Wheels; and EMESH is Environmental Monitoring, Ecological Sensor Hubs. Further details for the instrumentation are provided in the Supplementary Tables 1–3.

et al., 2020). Irrigation is the largest source of all water use by humans (Salmon et al., 2015) and application of irrigation increases evapotranspiration compared to non-irrigated agriculture (Mahmood and Hubbard, 2002; DeAngelis et al., 2010; Sorooshian et al., 2011).

Several field campaigns were conducted to better understand land-atmosphere (L-A) interactions (e.g., Kustas et al., 2005; Weckwerth et al., 2004). The Great Plains Irrigation Experiment (GRAINEX) is the first field campaign to investigate L-A interactions over irrigated and non-irrigated agricultural areas (Fig. 1). Specifically, GRAINEX's main purpose was to examine the L-A interactions, diurnal PBL evolution, changes in convective environment and precipitation over non-irrigated and irrigated agriculture (Rappin et al., 2021). In this paper we investigate the potential impacts of LULCC on a precipitation event that occurred within the GRAINEX study area on 23 July 2018. Note that the GRAINEX study area is part of the HPA region, which extends from Texas to South Dakota. The HPA includes Nebraska which is the most irrigated state in the US (USDA-ERS, 2021).

On 23 July 2018, a line of thunderstorms and convective precipitation was developed over the irrigated area. It reached its maximum over the boundary between the irrigated and non-irrigated land use and then dissipated when it entered the non-irrigated area (Fig. 2a-i). Specifically, the objective of this paper is to investigate the role of irrigated and non-irrigated land use on this precipitation event. To fulfill the objective, the Weather Research and Forecasting (WRF) model was used. Eight model simulations were conducted. They included systematic increases and decreases in soil moisture by 5 % and up to +15 % and −15 % compared to the control data over irrigated grid points. These changes reflect potentially different levels of irrigation applications and resultant soil moisture content. These simulations constitute seven experiments. An additional simulation was completed where irrigated land use was converted to grassland to determine the potential impacts of pre-irrigated pre-European settlement land cover. These 8 simulations will assist us in understanding L-A interactions under different levels of irrigation and land surface conditions.

The experimental design of utilizing a model simulation that reproduces an observed event as a control to conduct sensitivity analysis has been proposed by others in the past and has been used extensively (e.g., Nair et al., 1997; Chen et al., 2001; Holt et al., 2006; Niyogi et al., 2006; Lei et al., 2008; Schmid and Niyogi, 2017; Rodgers et al., 2018; Nair et al., 2019; Rappin et al., 2022). Thus, the approach used, and the analysis presented here is appropriate for this type of research question. The next sections discuss the experimental set-up, the results, and the paper is completed with a conclusions section.

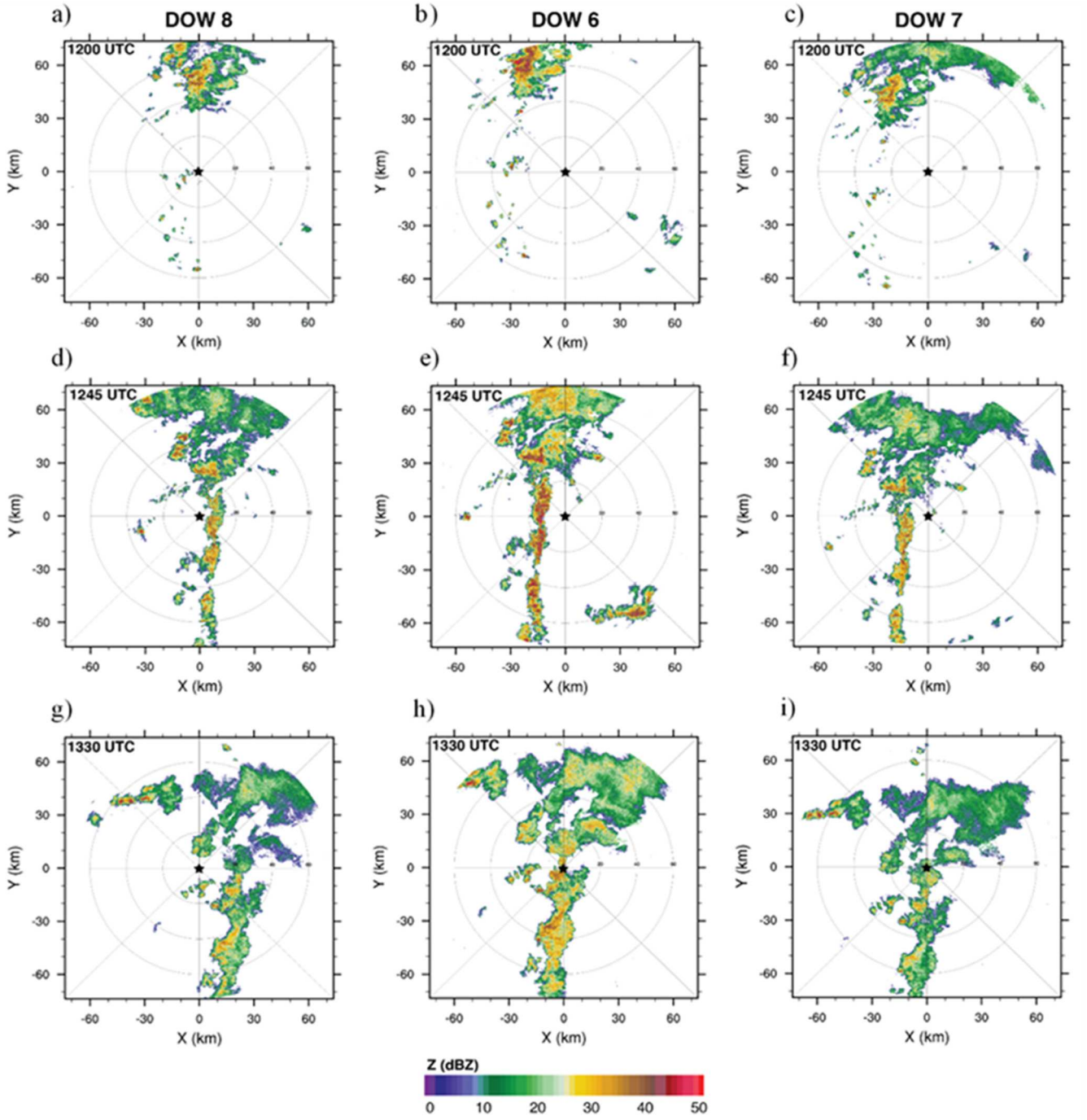

Fig. 2. a-i. Observed reflectivity from the DOW sites 6, 7, and 8. Instances are taken from a, b, c) at 1200 UTC; d, e, f) at 1245 UTC; g, h, i) at 1330 UTC. DOW is Doppler on Wheels.

2. Methods and data

2.1. The Weather Research and Forecasting (WRF) model and configuration

The Weather Research and Forecasting (WRF) model version 4.0 (Skamarock et al., 2019) was used for the purposes of this experiment. Initial and boundary conditions were provided by the North American Regional Reanalysis (NARR) (Mesinger et al., 2006) dataset. NARR data have a horizontal resolution of 32 km and extends through all North America. The USGS 24-category land use dataset was used to represent the land surface, which was already part of WRF's static land cover dataset. Subsequently, the Ozdogan and Gutman (2008) (https://sage.nelson.wisc.edu/data-and-models/datasets/) Irrigation Fraction dataset was implemented to more accurately capture irrigated land use (Whitesel, 2022). Fig. 3 shows the outer and inner domains for the experiments. The inner domain has a 4 km grid spacing and covers all of Nebraska and the outer domain has a horizontal grid spacing of 12 km and covers a large part of the central US (Fig. 3). The inner domain extends from 40° N 97° W to 43° N 104° W while the outer domain extends from 36° N 93° W to 46° N 106° W.

The Noah land surface model (Noah LSM) (Chen and Dudhia, 2001; Tewari et al., 2004) was used for the land surface physics parameterization. This model captures the important processes that occur at the

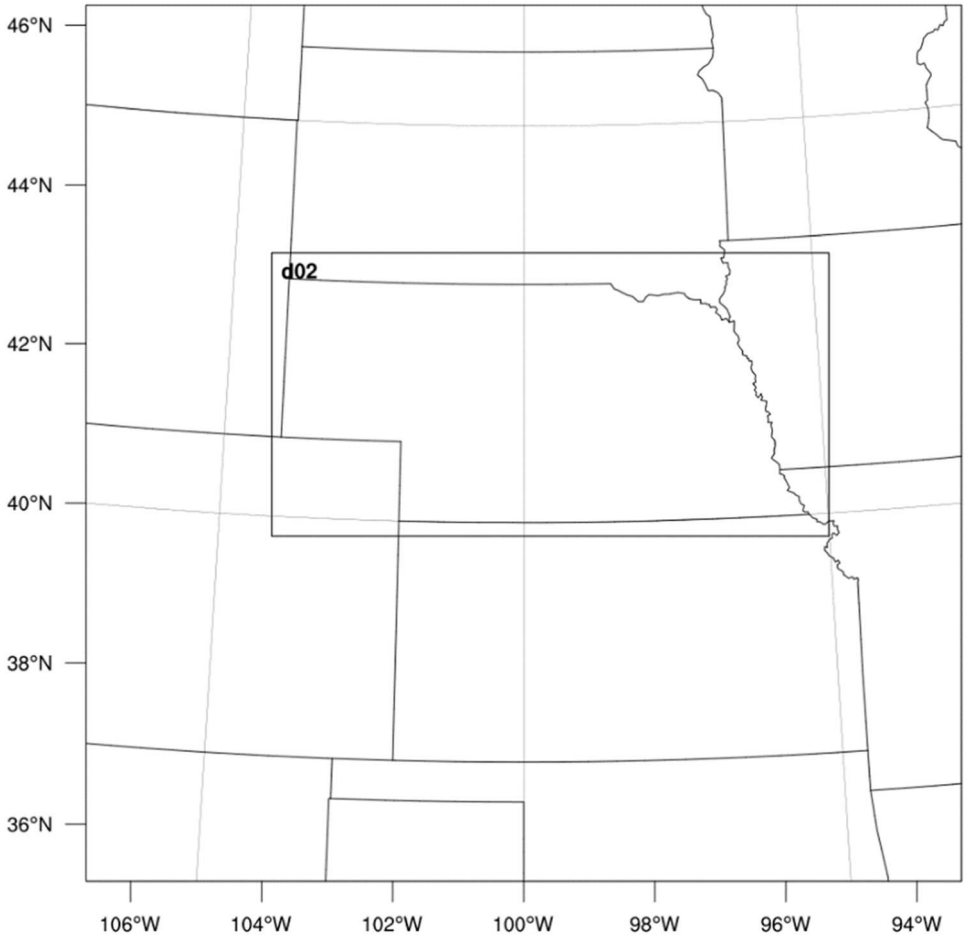

Fig. 3. Inner and outer domains for the WRF model applications.

surface, such as heat flux and evapotranspiration and includes vegetation parameters such as stomatal resistance, roughness length, leaf area index, and root depth for the simulation of surface moisture and energy budgets. The Noah LSM also features four soil depth levels, ranging from the surface to 1 meter below the surface, where precipitation can infiltrate at each of these levels. Soil moisture availability is determined by vegetation type and soil physical properties including heat capacity, field capacity, wilting point, and hydraulic conductivity. The Noah LSM determines the movement of moisture through the soil by gravitation pull, capillarity action, and transpiration. Numerous land use land cover studies have shown that the Noah LSM realistically represents the processes that occur at the Earth's surface (e.g., Mahmood et al., 2011; Winchester et al., 2017; Rodgers et al., 2018; Mahmood et al., 2020).

The Dudhia scheme (Dudhia, 1989) was used for shortwave radiation physics, and the RRTM scheme (Mlawer et al., 1997) for longwave radiation physics. These two schemes help to allocate radiative fluxes to the surface. The radiation calculations by these two schemes help calculate the surface energy balance for the model. The Yonsei University scheme (Hong et al., 2006) was used for boundary layer physics. The Yonsei scheme features non-local closure, and conducts calculations such as the diffusion of heat, momentum, and moisture. The Goddard microphysics (Tao et al., 1989; Tao et al., 2016) scheme was used to parameterize cloud microphysics. The Goddard scheme is a cloud-scale single moment 6-class scheme. Cloud microphysics schemes provide non-convective precipitation to the surface and provide cloud effects for the radiation schemes to handle.

Though only applied to the outermost domain, the Kain-Fritsch cumulus scheme (Kain, 2004) was used to parameterize processes that involve convective clouds. The low resolution of the outer domain necessitates a cumulus scheme to resolve the updrafts that may occur at sub-grid levels. A summary of the model physics parameterization schemes selected for this research is presented in Table 1.

Table 1
Summary of model physics and configurations for the applications.

Model and physics parameterizations used	References
WRF Version	4.0
Grid Increment	12 km (outer domain), 4 km (inner domain)
Model Simulation Time	0600 UTC July 22, 2018 – 0600 UTC July 24, 2018
Initial and Boundary Conditions	NARR
Land Use	USGS 24-class + Ozdogan Irrigation Fraction (Ozdogan et al., 2010)
LSM	Noah (Chen and Dudhia, 2001; Tewari et al., 2004)
Vertical Layers	35
Boundary and Surface Layer	Yonsei (Hong et al., 2006)
Cloud Microphysics	Goddard (Tao et al., 1989, 2016)
Cumulus Parameterization Scheme	Kain-Fritsch (outer domain only) (Kain, 2004)
Shortwave Radiation	Dudhia (Dudhia, 1989)
Longwave Radiation	RRTM (Mlawer et al., 1997)

These parameterization schemes were selected after several sensitivity tests using different model configurations, including, the Mellor-Yamada-Janjic (Mesinger, 1993; Janjic, 1994) and the Single Moment 6-class microphysics (Hong and Lim, 2006) parameterization schemes. However, inclusion of these schemes produced lower amounts of

Table 2
Irrigation experiments.

Experiment Name	Irrigation/Soil Moisture Sensitivity
CTRL	None
WET05	+5 %
WET10	+10 %
WET15	+15 %
DRY05	−5 %
DRY10	−10 %
DRY15	−15 %
GRASS	None

precipitation. In addition, a 12-hour and a 6-hour dynamic adjustment periods were implemented but they produced unsatisfactory results as well. After these tests 24-hr dynamic adjustment period was chosen because it produced the most satisfactory results compared to radar observed precipitation.

2.2. Experiments

To better simulate the impacts of irrigation on the precipitation event during GRAINEX, the Irrigation Fraction dataset of the Ozdogan and Gutman (2008) was implemented for all model runs. An algorithm was created to adjust land use tiles to irrigated agriculture across both WRF domains. First, the Irrigation Fraction dataset was regridded onto the same grid as the WRF domain, then it was compared to the land use categories within the WRF input files. If the irrigation fraction dataset identified a grid point with 50 % or greater irrigation fraction, it was defined as irrigated land within the WRF input files for that specific grid point. As noted previously, soil moisture was systematically increased and decreased from the CTRL data by 5 % and up to +15 % and −15 %, over irrigated areas (Table 2). These changes reflect different levels of soil moisture in the presence of irrigation. Moreover, the changes in soil moisture were applied to all depths. An additional simulation was completed to determine the impacts of grassland assuming that the irrigation was replaced with grassland, to simulate pre-irrigation land use and its impacts.

After implementation of the Ozdogan and Gutman (2008) dataset, the land use of the inner domain (entire state of Nebraska) is a mix of grassland (36.07 %), followed by rainfed agriculture (33.81 %). Irrigated agriculture and cropland/grassland mosaic represent 16.77 % and 11.95 % of the land use land cover, respectively. However, it is also clear from Fig. 1 that the presence of irrigation is quite extensive in southeastern Nebraska and a distinct land use boundary exists between irrigated and non-irrigated land uses. To further understand the influence of irrigated and non-irrigated uses, two different areas (identified by blue and red boxes) (Fig. 1) have been selected for detailed analyses, which represent irrigated and non-irrigated land use.

2.3. Control simulation

Assessment of the model performance was conducted by comparing data from the simulations and the 12 Integrated Surface Flux System (ISFS) stations that were deployed during the GRAINEX field campaign (Fig. 1) (Earth Observing Laboratory, 2020). These stations were distributed over both irrigated and non-irrigated land use, with six sites deployed in the irrigated area, and six sites deployed in the non-irrigated area (Fig. 1). The ISFS stations observed variables such as air temperature, dew point temperature, and sensible and latent heat flux. Observations for these variables were compared to the modeled estimates. Three statistical measures of model performance were used including the coefficient of determination (r^2), the root mean square error (RMSE), and the mean absolute error (MAE) (Legates and McCabe, 1999).

Table 3 shows these statistics for 2 m air temperatures, sensible heat fluxes, and latent heat fluxes. The model performed satisfactorily in reproducing 2 m air temperatures (Table 3) with r^2 values up to 0.97 and RMSE and MAE values as low as 1.33 and 1.09 °C, respectively. Model evaluation statistics show that the model reproduced latent heat flux better than sensible heat flux for both irrigated and non-irrigated agriculture (Fig. 4a-b). Sensible heat flux had r^2 values as high as 0.93 and RMSE and MAE values as low as 44.81 and 29.01 W m^{-2}, respectively (Table 3). However, these values reached as high as 173.42 and 107.57 W m^{-2} for the latter two statistics. Latent heat flux assessment shows r^2 as high as 0.95 and RMSE and MAE as low as 50.86 and 29.62 W m^{-2}, respectively. Though r^2 values for both fluxes were comparable, the RMSE and MAE values were considerably high. In addition, diurnal latent and sensible heat flux variations were captured by the control simulation.

For precipitation, the control simulation shows a line of storms were initiated (Fig. 2) over the irrigated cropland (northcentral part of the study domain; Fig. 1). When these storms started to propagate over the area dominated with the non-irrigated land use, they weakened and dissipated. Precipitation for the event was concentrated on the irrigated side, with a value of 42.1 mm (Table 4; small box of Fig. 5a). The area average (blue box of Fig. 1) value is 0.88 mm for the entire 24 hr period. For the non-irrigated side (red box of Fig. 1), a trace amount of precipitation was simulated (Table 5).

To ensure that the simulation of the convective event was acceptable, model reflectivity was compared to the observed reflectivity of the DOW sites (Fig. 5a-b). It was found that the model slightly underestimated the reflectivity, and thus, the intensity of rainfall; and placed precipitation slightly west of the actual event. The modeled precipitation appeared around an hour and a half later, at 1500 UTC, compared to observations. Despite these small biases, we suggest that the overall model performance was acceptable for the current application.

Furthermore, we have compared modeled and radiosonde observations during the GRAINEX field campaign. Fig. 6a-b compares the 1300

Table 3
Model performance statistics based on hourly timeseries (developed from 5-minute data for 06:00 UTC July 23, 2018 to 06:00 UTC July 24, 2018).

Statistics	Site 1	Site 2	Site 3	Site 4	Site 5	Site 6	Site 7	Site 8	Site 9	Site 10	Site 11	Site 12
Air Temperature (°C)												
RMSE (°C)	2.61	2.17	2.20	2.19	2.12	1.39	1.65	1.33	2.31	2.19	2.11	2.13
r^2	0.60	0.71	0.74	0.75	0.77	0.92	0.84	0.94	0.86	0.92	0.89	0.97
MAE (°C)	2.20	1.96	1.82	1.81	1.83	1.15	1.37	1.09	2.17	1.88	1.89	1.83
Sensible Heat Flux H (W m^{-2})												
RMSE (W m^{-2})	44.81	97.44	69.36	88.59	92.11	79.88	67.43	95.83	146.94	172.01	85.16	173.42
r^2	0.75	0.92	0.63	0.27	0.30	0.80	0.66	0.49	0.78	0.66	0.93	0.82
MAE (W m^{-2})	29.01	62.80	46.08	56.72	57.33	53.58	45.96	53.04	87.64	100.33	57.36	107.57
Latent Heat Flux (W m^{-2})												
RMSE (W m^{-2})	75.39	50.86	74.95	79.61	67.57	45.54	82.94	87.84	63.92	101.37	53.07	98.80
r^2	0.82	0.42	0.78	0.71	0.77	0.92	0.67	0.63	0.87	0.88	0.95	0.88
MAE (W m^{-2})	47.28	29.62	37.86	38.51	35.91	30.60	52.29	58.17	42.48	66.68	35.69	67.20

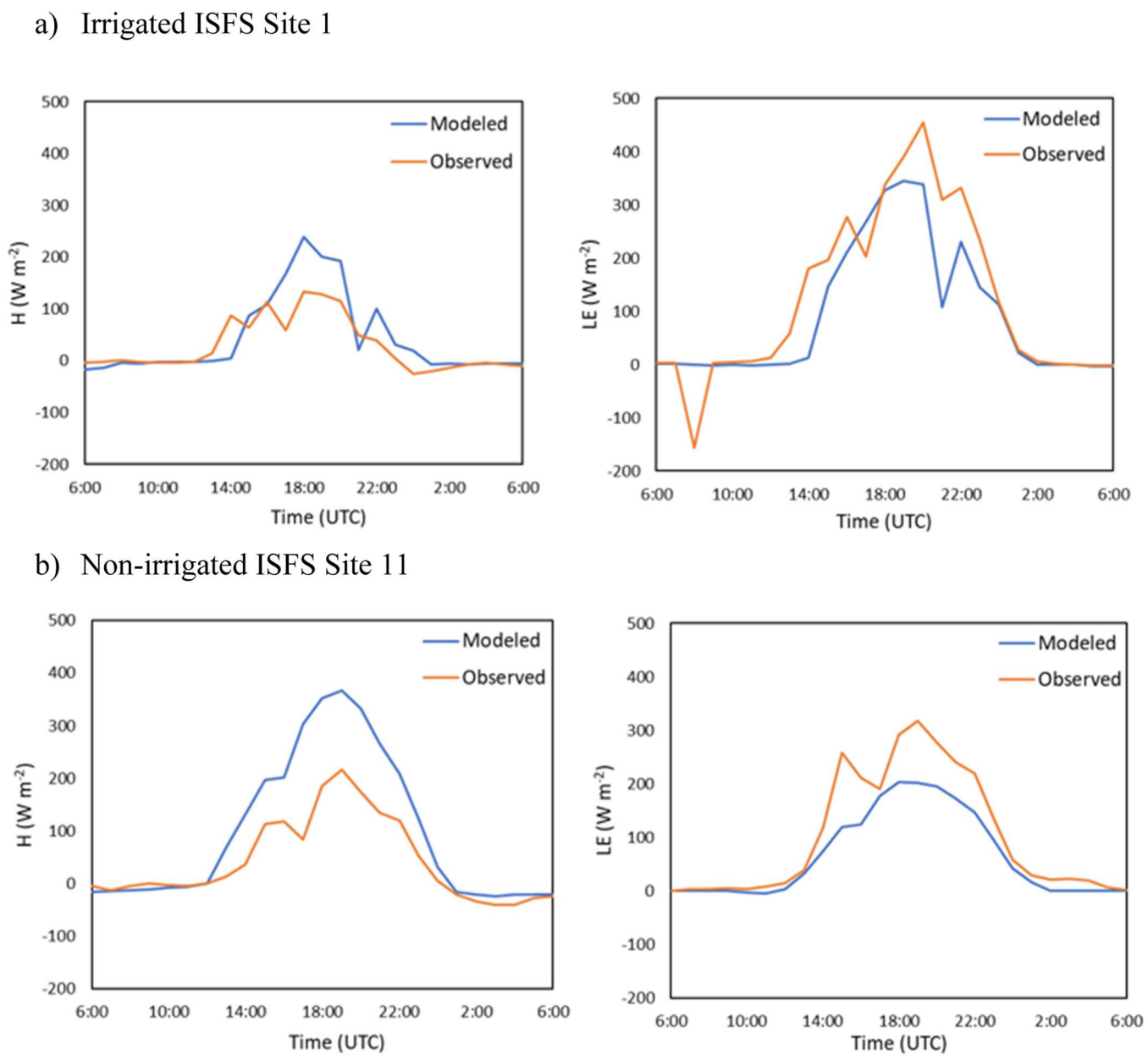

Fig. 4. a-b. Observed and modeled latent (LE) and sensible (H) heat flux from: a) irrigated and b) non-irrigated locations for 06:00 UTC July 23, 2018 to 06:00 UTC July 24, 2018).

Table 4
Simulated precipitation for the convective event at 1500 UTC, 23 July 2018 (shown by smaller box within Fig. 5a).

Simulation	Precipitation (mm)
CTRL	42.1
WET05	18.0
WET10	11.4
WET15	22.4
DRY05	88.2
DRY10	31.3
DRY15	33.1
GRASS	149.4

UTC 23 July 2018, soundings from both the model and the ISS observations from the York Airport and the Rogers Farm. At York, from the surface to 700 mb level, the observed sounding temperature ranged from 21.2 to 9.5 °C while the modeled sounding temperature ranged from 19.1 to 8.5 °C. While at Rogers Farm, from the surface to 700 mb level, the observed sounding temperature ranged from 21.0 to 8.9 °C while the modeled sounding temperature ranged from 20.8 to 9.3 °C. Near surface dew point temperature profiles are drier in the simulations compared to the observations. The observed dew point temperature at York ranged between 20.4 to 4.9 °C from the surface to 700 mb level while it ranged between 17 and 7 °C for the modeled estimates. At Rogers Farm, observed dew point temperature ranged between 20.1 to 4.2 °C from the surface to 700 mb level. The range for the modeled dew point temperature for Roger Farm from the surface to 700 mb level was 18.3 to 6.6 °C. In summary, the pattern of temperature and dew point temperature changes with height are generally comparable between the model and observations.

Based on these findings, it is concluded that the overall model performance was acceptable for this analysis.

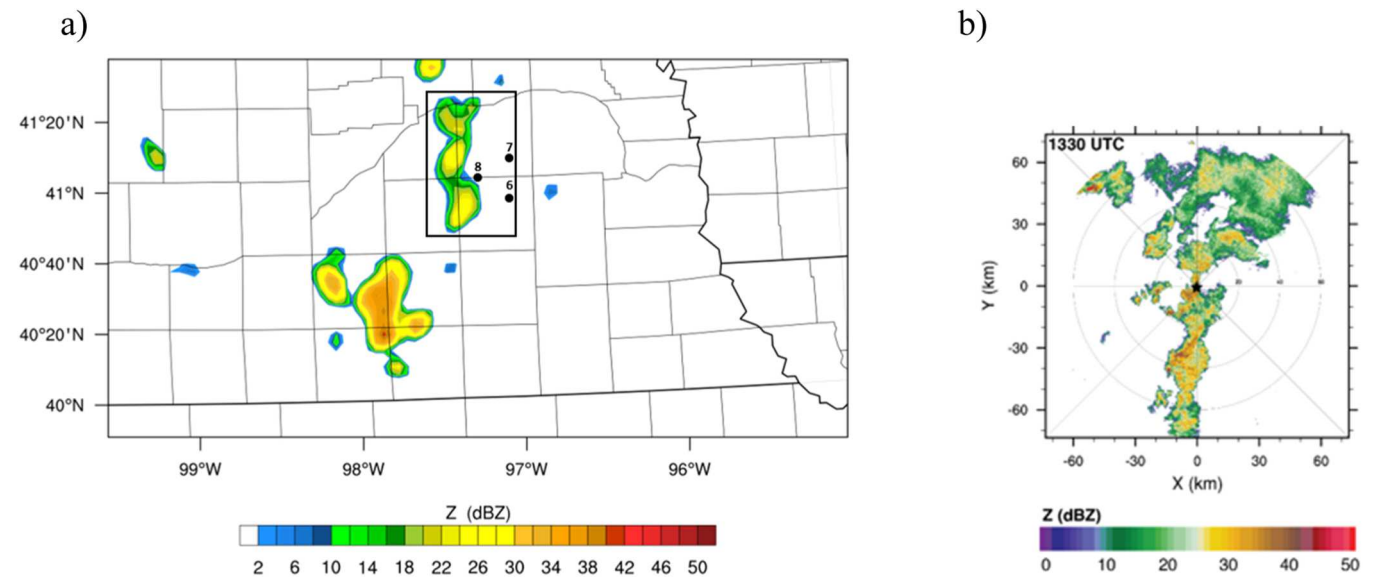

Fig. 5. a-b. Comparisons of reflectivity with: a) the model reflectivity at 1500 UTC, 23 July 2018 and b) the DOW 6 reflectivity at 1330 UTC, 23 July 2018. Small dots within the smaller box represent DOW sites. DOW is Doppler on Wheels.

Table 5
Modeled planetary boundary layer variables for irrigated, non-irrigated, and grassland areas for 06:00 UTC July 23, 2018 to 06:00 UTC July 24, 2018. Soil moisture was not changed over non-irrigated areas and grassland. Abbreviations are as follows: T is 2 m air temperature, T_E is 2 m equivalent temperature, H is sensible heat flux, LE is latent heat flux, PBLH is planetary boundary layer height, and p is precipitation.

	Statistic	T (°C)	T_E (°C)	H (W m^{-2})	LE (W m^{-2})	PBLH (m)	p (mm)
Irrigated							
CTRL	Max	32.7	63.2	490	426	1977	8.4
	Min	16.4	41.7	−41	−18	0	T
	Mean	23.6	53.5	66	88	535	0.9
WET05	Max	32.5	64.4	493	452	1687	7.2
	Min	16.5	44.2	−42	−18	0	T
	Mean	23.3	53.8	55	100	486	0.8
WET10	Max	32.4	65.0	493	492	1926	6.
	Min	16.5	44.2	−42	−18	0	T
	Mean	23.2	54.3	50	104	453	0.5
WET15	Max	32.2	65.5	494	525	1937	6.5
	Min	16.3	43.9	−43	−18	0	T
	Mean	23.2	54.5	48	113	469	0.3
DRY05	Max	34.5	63.2	526	439	2198	4.5
	Min	15.9	41.3	−44	−21	0	0
	Mean	24.2	52.8	102	40	625	0.2
DRY10	Max	34.8	63.9	546	461	2516	1.0
	Min	14.9	37.6	−50	−27	0	0
	Mean	24.0	52.3	108	28	640	0.1
DRY15	Max	34.8	62.9	544	465	2537	5.7
	Min	14.8	39.0	−51	−28	0	0
	Mean	24.0	52.0	111	29	653	0.5
Non-Irrigated							
	Max	33.8	64	513	361	1982	0.2
	Min	15.4	42.5	−45	−20	0	0
	Mean	24.3	53.7	99	56	634	T
Grassland							
	Max	32.7	64.7	486	422	1706	12.6
	Min	16.5	43.9	−42	−18	0	Trace
	Mean	23.6	53.9	67	77	517	3.2

3. Results & discussion

Here we discuss the impacts of the three land use categories, including, irrigated, non-irrigated, and grassland, on precipitation, latent and sensible heat flux, planetary boundary layer height, vertical distribution of equivalent potential temperature, and near surface air and equivalent temperature. Soil moisture changes were made only over irrigated areas assuming different levels of irrigation, which allowed us to assess their potential impacts. Thus, assessment for irrigated land use includes impacts of various levels of soil moisture (WET05, WET10, WET15, DRY05, DRY10, and DRY15) and discussion on both irrigated and grassland land use is presented as experiment minus control (EXP-CTRL). As noted previously, the model simulations were conducted for 48 h, with the first 24-hour period as a dynamic adjustment or initialization period. Hence, the results will focus on the second 24-hour period, from 0600 UTC (0000 LST) 23 July 2018 to 0600 UTC (0000 LST) 24 July 2018, which covers the day when the precipitation event occurred. Results presented here include analyses from 1500 UTC (time of precipitation) and from the entire 24-hr. period. Note that 1500 UTC is the modeled timing of precipitation while the assessment of the 24-hr. period provides additional perspective of overall impacts of irrigated and non-irrigated land use on the atmosphere. For precipitation related discussions, we focused on the area shown by the smaller box within Fig. 5a. The area average values for the rest of the variables correspond to areas within the blue and the red 'boxes' in Fig. 1. Again, these analyses contribute to the understanding of the overall conditions in the study area.

3.1. Irrigated land-use

3.1.1. Precipitation

As noted previously, the CTRL simulation produced 42.1 mm of precipitation (Fig. 5a; smaller box). Subsequent simulations show that precipitation is sensitive to changes in irrigation and soil moisture (Fig. 7a-f). At 1500 UTC with increasing soil moisture in the irrigated areas, it appears that the precipitation amount declines. Precipitation for the WET experiments (within the smaller box of Fig. 5a) is 18, 11.4, and 22.4 mm (a 24.1, 30.7, and 19.7 mm decrease compared to CTRL) for the WET05, WET10, and WET15 simulations, respectively

(Table 4). Precipitation for the DRY experiments is 88.2, 31.3, and 33.1 mm (a 46.1 increase, and 10.8 and 9.0 mm decrease compared to

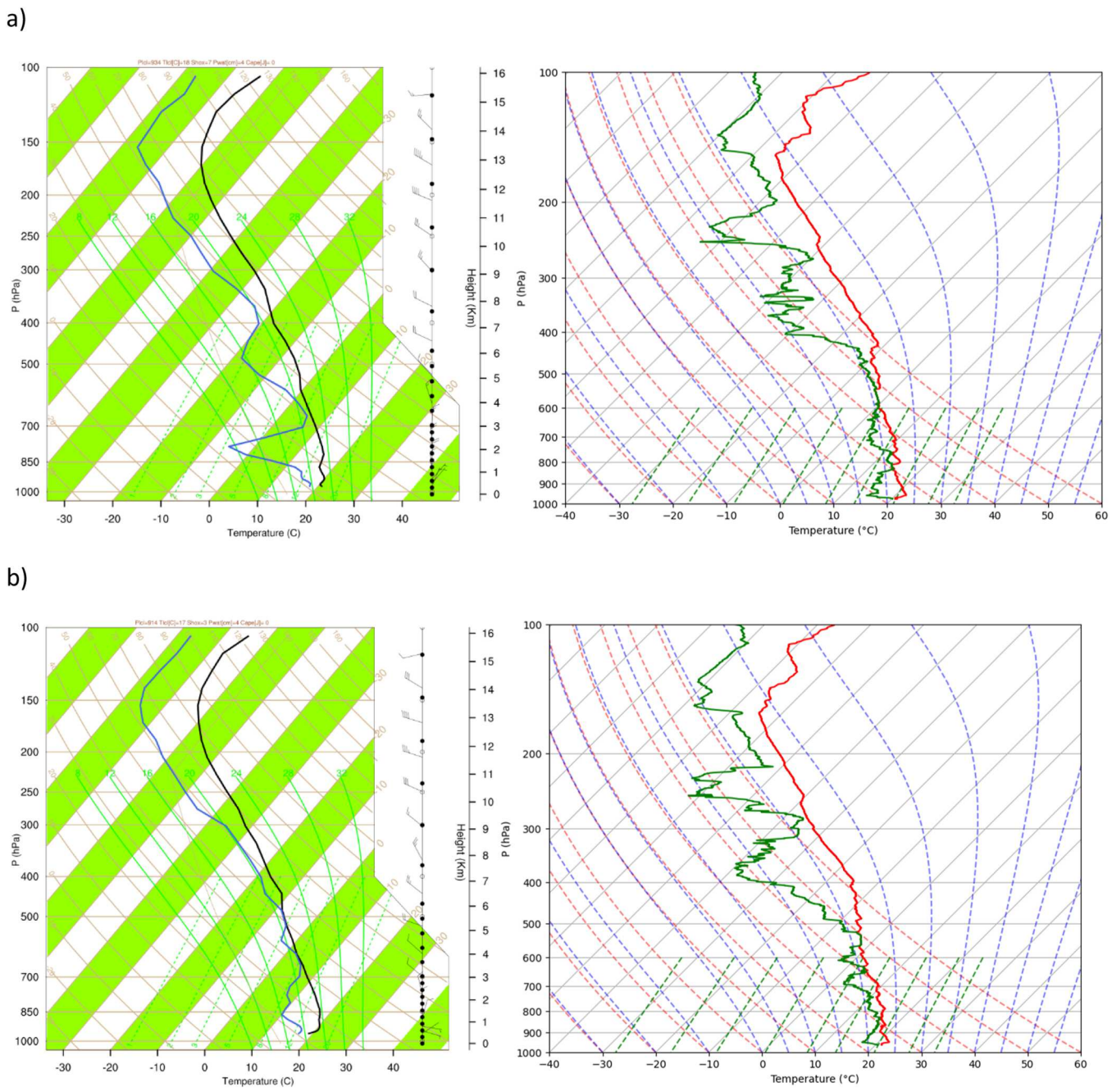

Fig. 6. a-b. Comparison of model soundings (left) to observed soundings (right) for: a) York (ISS 3) and b) Rogers Farm (ISS 2) for 1300 UTC July 23, 2018.

CTRL) for the DRY05, DRY10, and DRY15 simulations, respectively (Table 4).

In addition, area average 24 hr. precipitation for the WET experiments is 0.8, 0.5, and 0.3 mm (a 0.1, 0.4, and 0.6 mm decrease compared to CTRL) for the WET05, WET10, and WET15 simulations, respectively (Table 4). Average precipitation for the DRY experiments is 0.2, 0.1, and 0.5 mm (a 0.7, 0.8, and 0.4 mm decrease compared to CTRL) for the DRY05, DRY10, and DRY15 simulations, respectively (Table 5). Thus, different levels of irrigation water applications in WRF impacted precipitation amounts for the 23 July 2018 event.

3.1.2. *Latent heat flux*

Latent and sensible heat flux play an important role in the development of convection (Mahmood et al., 2011; Sen Roy et al., 2011; Suarez et al., 2014; Winchester et al., 2017; Rodgers et al., 2018). Impacts on latent heat flux due to modeled changes in soil moisture are clear (Fig. 8a-f). Increases (decreases) in soil moisture resulted in increases (decreases) in latent heat flux. For example, in the areas of precipitation, latent heat flux increases about 50, 100, and 150 W m^{-2} for the WET05, WET10, and WET15, respectively (Fig. 8a-c) compared to CTRL at 1500 UTC. For DRY simulations, latent heat flux declines up to 50 W m^{-2} (Fig. 8d-f). Thus, the WET experiments show increases in latent heat flux at 1500 UTC. The DRY experiments show decrease in latent heat flux at 1500 UTC.

Area average latent and sensible heat flux and planetary boundary layer height (PBLH) are shown in Fig. 9a-c. It is found that, overall, area average latent heat fluxes for the day decreased by 48, 60, and 59 W m^{-2} for the DRY05, DRY10, and DRY15 simulations, respectively (Table 5 and Fig. 9a). Area average latent heat flux increased by 12, 16, and 25 W m^{-2} for the WET05, WET10, and WET15 simulations, respectively

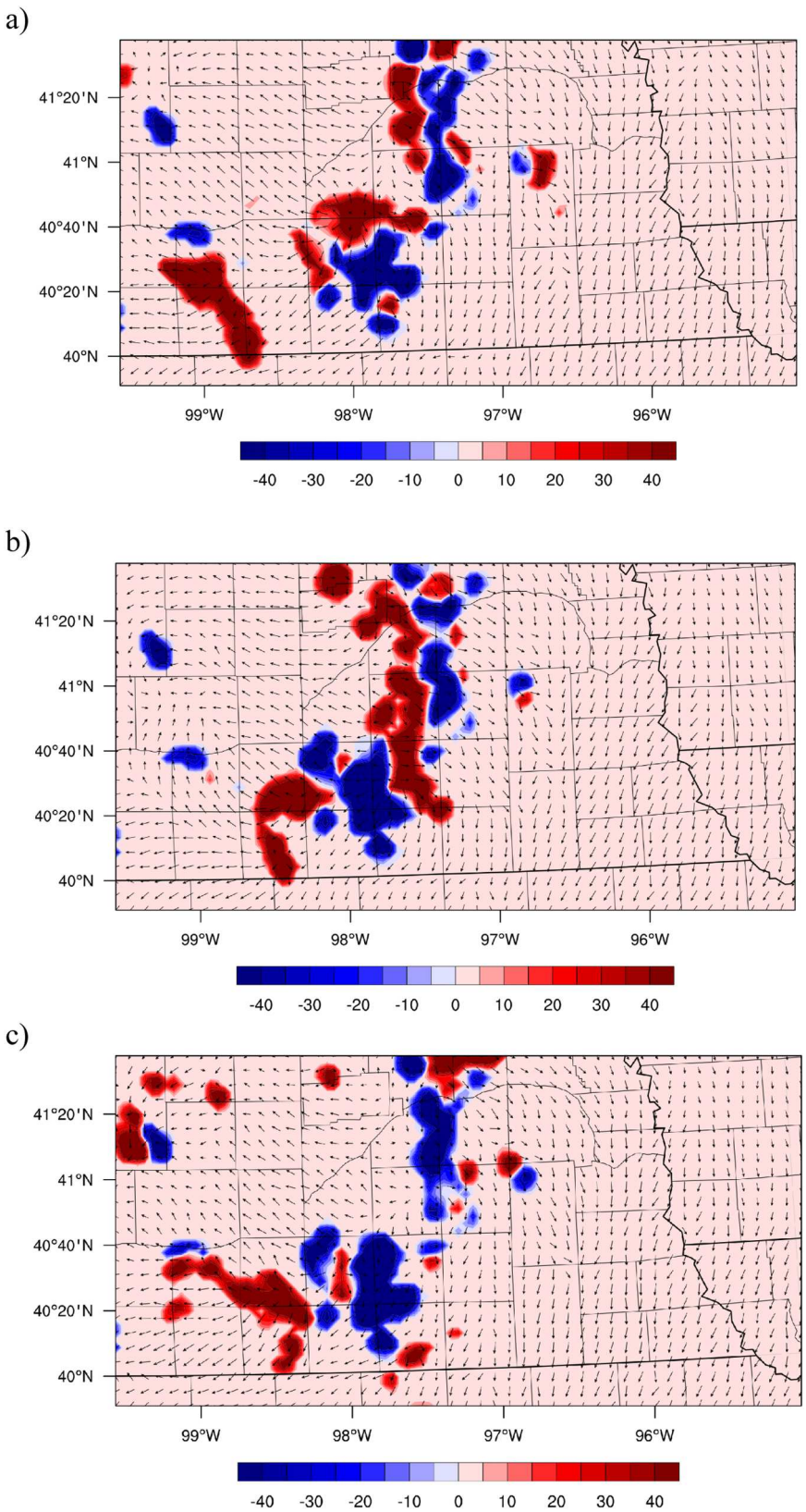

Fig. 7. a-f. EXP – CTRL plots of reflectivity (dBZ) at 1500 UTC, 23 July 2018 for: a) WET05, b) WET10, c) WET15, d) DRY05, e) DRY10, and f) DRY15.

(Table 5). This means that, compared to CTRL, latent heat flux could increase up to 28 % over irrigated cropland due to increased irrigation (Table 5). Average latent heat flux values for the DRY simulations are at 40, 28, and 29 W m^{-2} for the DRY05, DRY10, and DRY15 simulations (48, 60, and 59 W m^{-2} decrease, compared to CTRL), respectively. In other words, compared to CTRL, latent heat flux decreases up to 67 %

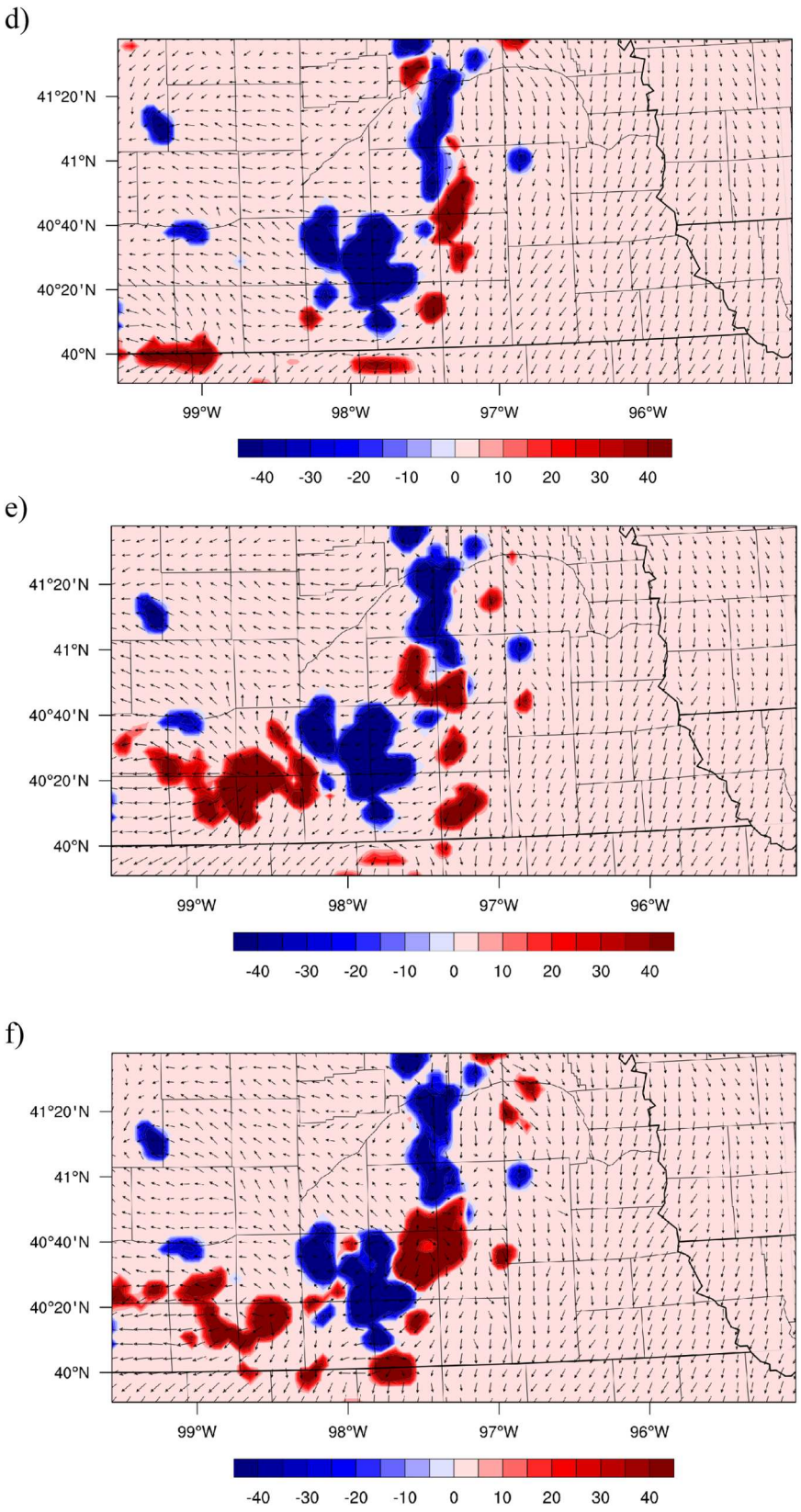

Fig. 7. (*continued*).

when irrigation is removed (Table 5).

3.1.3. *Sensible heat flux*

Changes to soil moisture have an opposite effect with sensible heat flux. In this case, soil moisture increases (decreases) result in decreases (increases) in sensible heat flux. For WET05, WET10, and WET15 simulations and compared to CTRL, sensible heat flux declines from 50 to 100 W m^{-2} in the areas of precipitation at 1500 UTC. On the other hand,

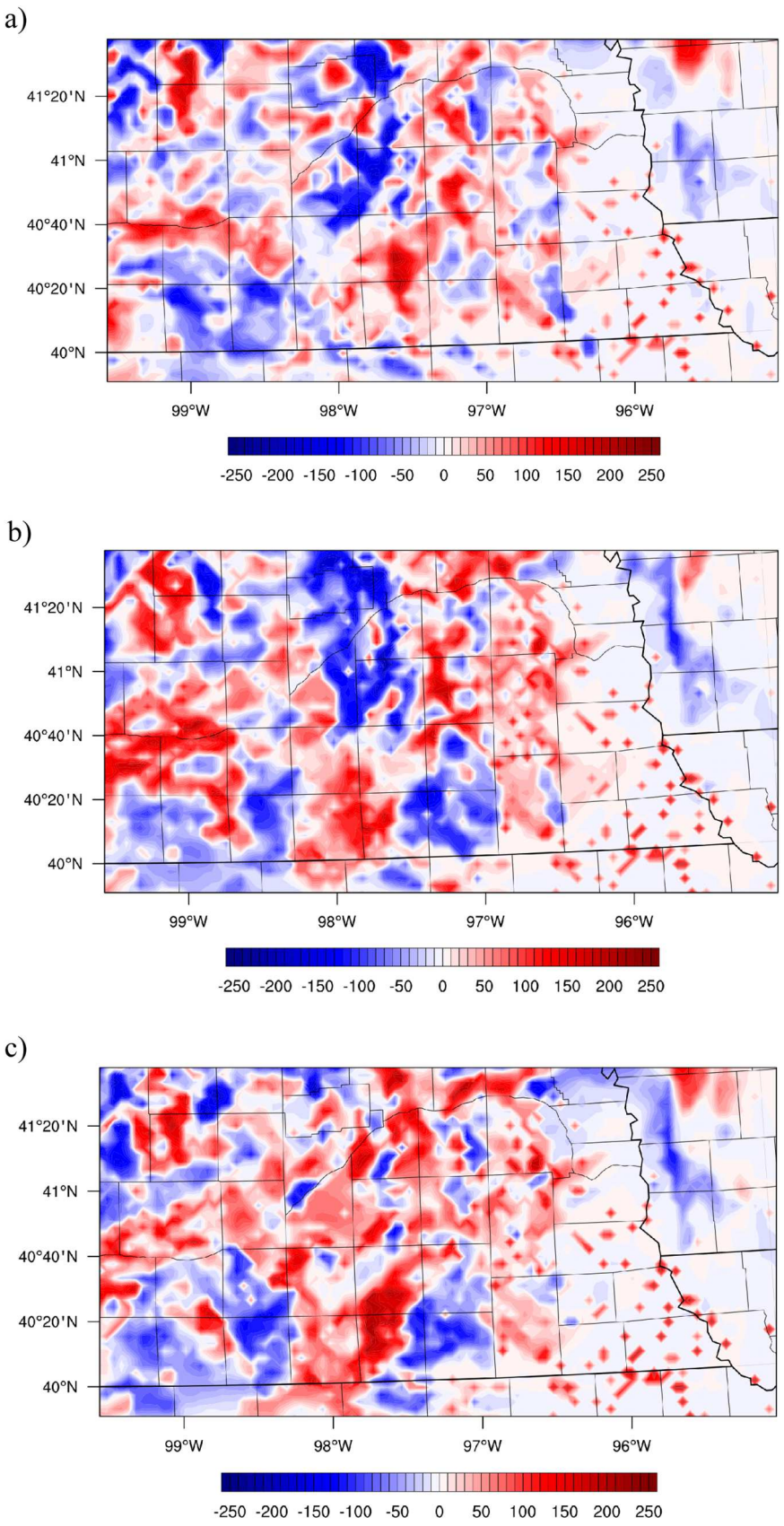

Fig. 8. a-f. EXP-CTRL latent heat flux (W m^{-2}) at 1500 UTC, 23 July 2018 for: a) WET05, b) WET10, c) WET15, d) DRY05, e) DRY10, and f) DRY15.

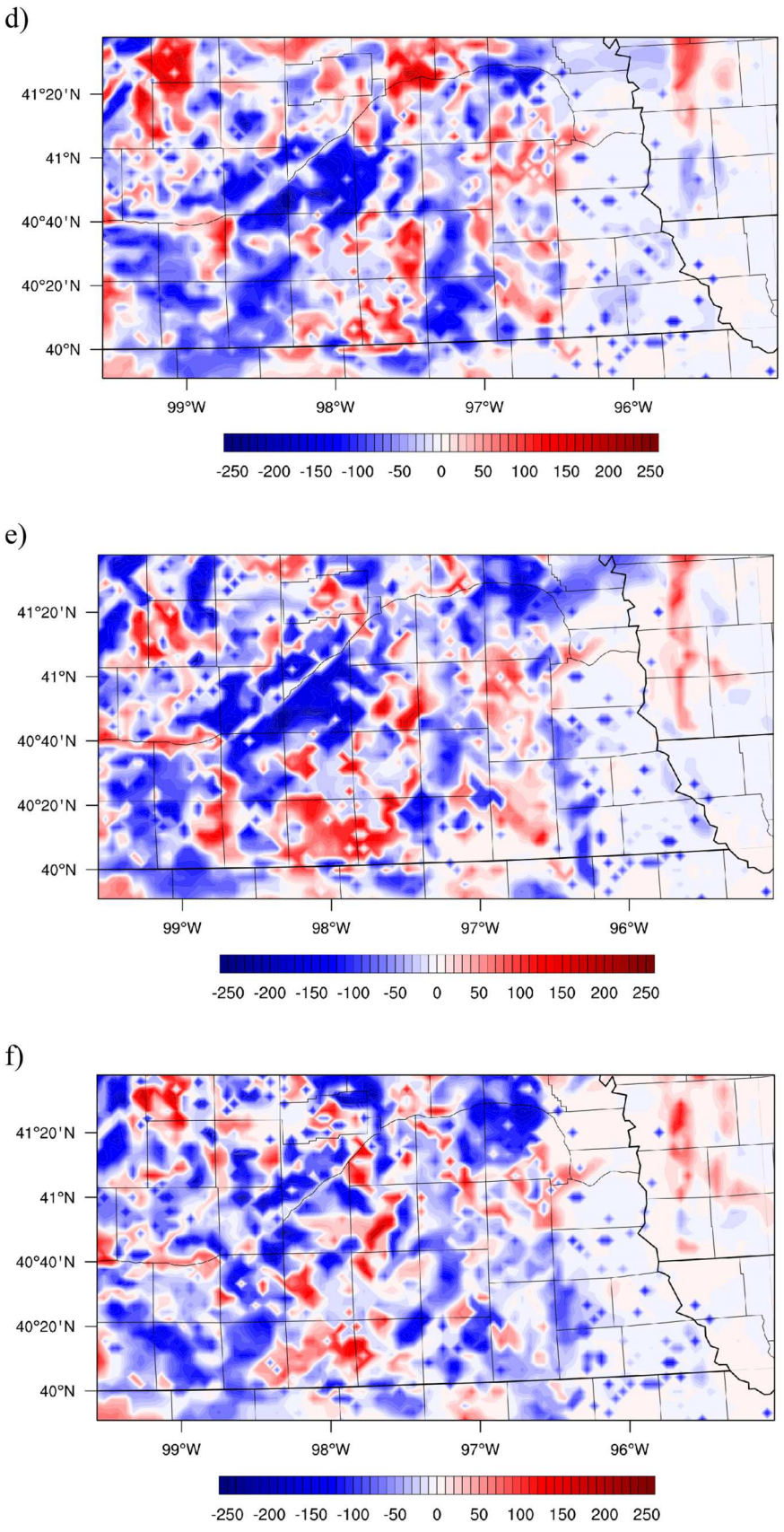

Fig. 8. (*continued*).

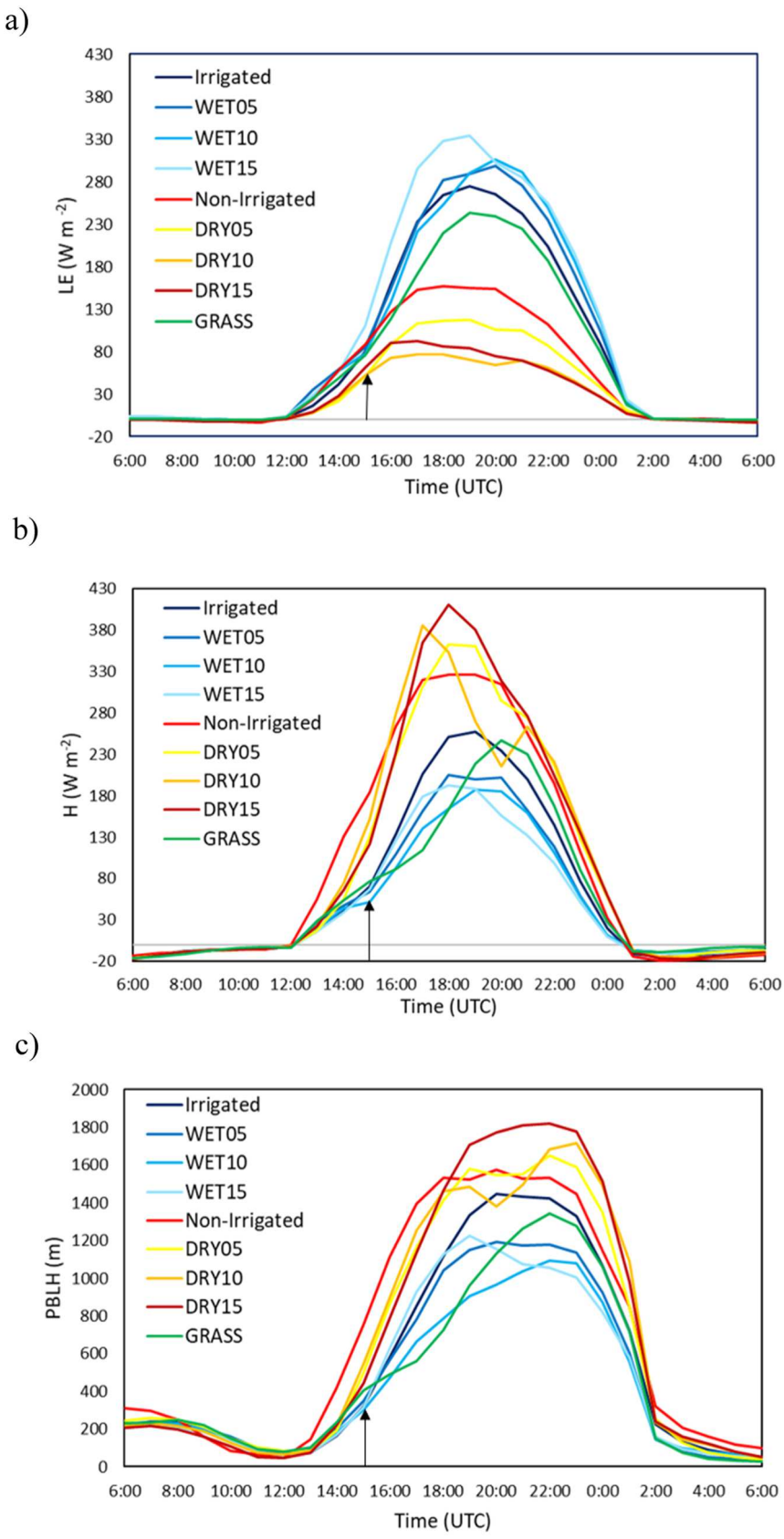

Fig. 9. a-c. Area average hourly: a) latent heat flux, b) sensible heat flux, and c) planetary boundary layer height for all simulations on 23 July 2018. Arrows indicate the time of precipitation.

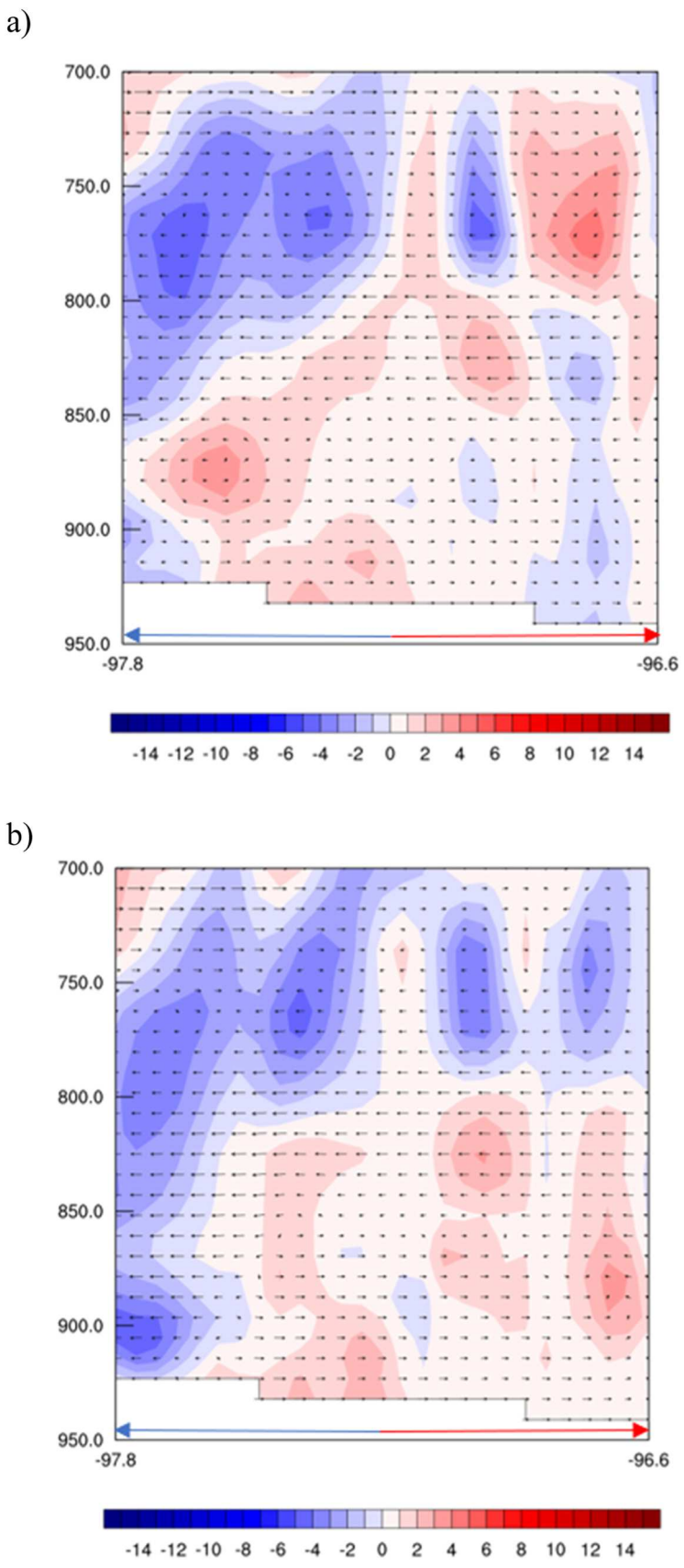

Fig. 10. a-f. EXP-CTRL equivalent potential temperatures (K) from a vertical cross section (40.94° N Latitude) at 1500 UTC, 23 July 2018 for: a) WET05, b) WET10, c) WET15, d) DRY05, e) DRY10, and f) DRY15. Arrows delineate irrigated (blue arrow) and non-irrigated (red arrow) land.

c)

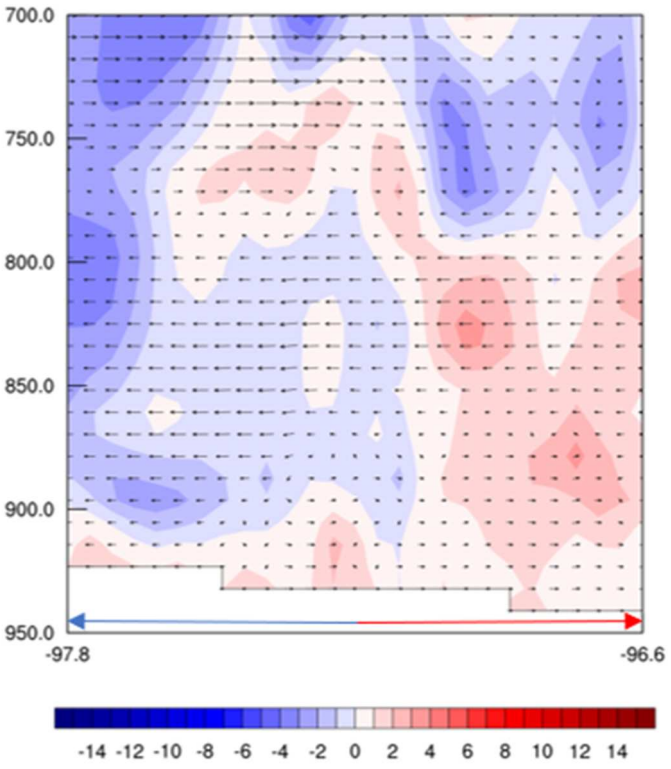

d)

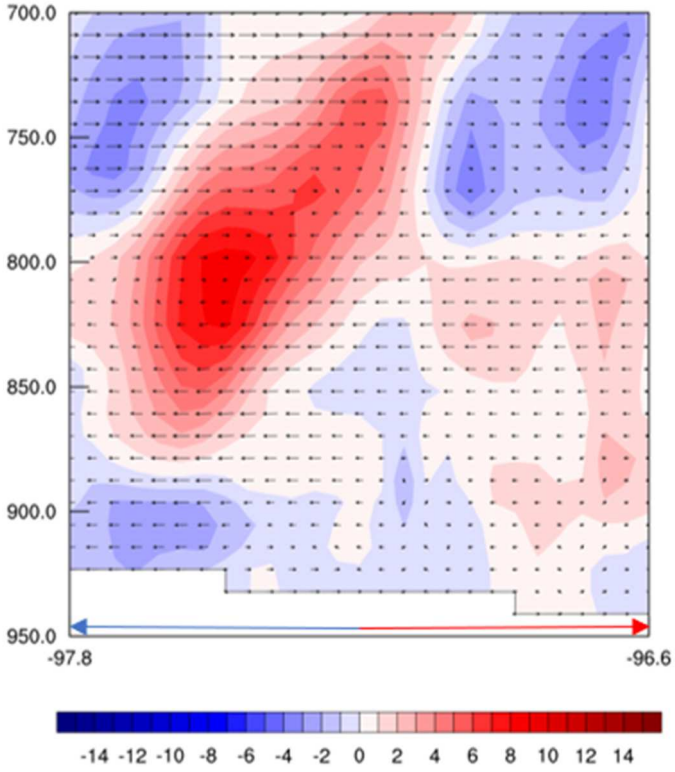

Fig. 10. (*continued*).

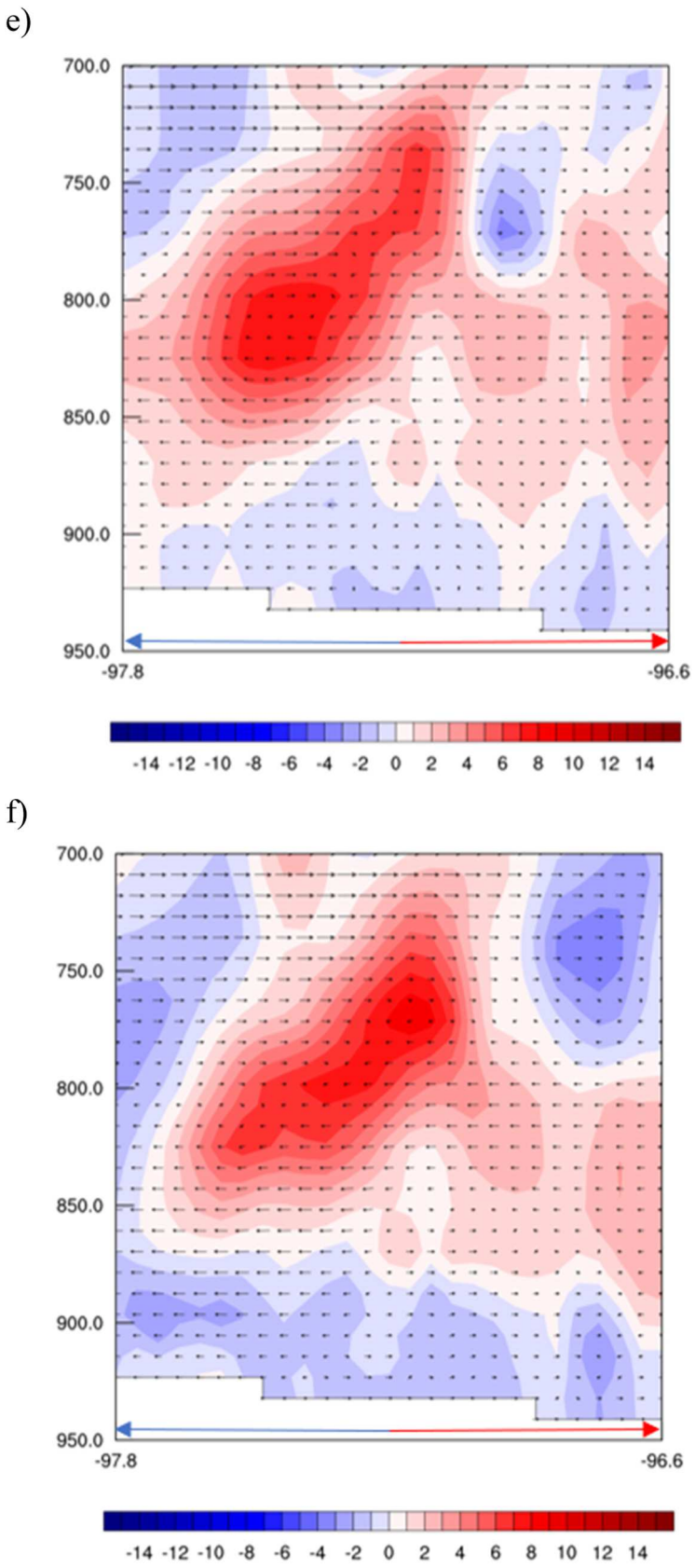

Fig. 10. (*continued*).

sensible heat flux increase >200 W m^{-2} for DRY simulations in the vicinity of precipitation. In short, the WET and DRY experiments show decreases and increases in sensible heat flux at 1500 UTC, respectively.

Overall, area average sensible heat flux values for the WET experiments are at 55, 50, and 48 W m^{-2}. Thus, compared to CTRL, sensible heat flux decreases by 11, 16, 18 W m^{-2} for the WET05, WET10, and

WET15, respectively (Table 5 and Fig. 9b). This also means that average sensible heat flux can decrease up to 27% compared to CTRL (Table 5). Area average sensible heat flux are 102, 108, 111 W m^{-2} for the DRY05, DRY10, and DRY15 simulations, respectively. Hence, sensible heat flux increases by 36, 42, and 45 W m^{-2} for these simulations, respectively (Table 5). Furthermore, compared to CTRL, average sensible heat flux increased by up to 68% when irrigation was removed (Table 5).

3.1.4. Planetary boundary layer height

Irrigation and resultant changes to soil moisture also influence the development of the planetary boundary layer (Quintanar et al., 2008; Mahmood et al., 2011; Leeper et al., 2011, Suarez et al., 2014). It is found that more irrigation, represented by increased soil moisture, decreases PBLH, and vice versa with reduced soil moisture. Irrigated areas have a shallower (~ 100 m) planetary boundary layer than their non-irrigated counterparts during the precipitation event at 1500 UTC.

The WET experiments found, overall, area average PBLH values of 486, 453, and 469 m (49, 82, and 66 m lower compared to CTRL) for the WET05, WET10, and WET15 simulations, respectively. Thus, increased irrigation and soil moisture reduce PBLH by up to 16 % compared to CTRL (Table 5 and Fig. 9c). The DRY experiments simulate average PBLH values at 625, 640, and 653 (a 90, 105, and 118 m higher compared to CTRL) for the DRY05, DRY10, and DRY15 simulations, respectively (Table 5). Removing irrigation resulted in up to a 22 % increase in PBLH compared to CTRL (Table 5). We suggest that higher latent (sensible) heat flux over irrigated (non-irrigated) areas limit (enhance) the growth of the PBLH.

3.1.5. Vertical distribution of equivalent potential temperature

Equivalent potential temperature (θ_e) is a measure of moist static energy (Eltahir, 1998; Pielke, 2001). Warmer and moister air has higher equivalent potential temperatures compared to cooler and drier air. Fig. 10a-f shows cross section of θ_e for 41.94° latitude, surface to 700 mb pressure level, and includes a significant portion of both irrigated and non-irrigated land use land cover. Compared to CTRL, the WET experiments show lower θ_e aloft but higher θ_e over the lower atmosphere for the irrigated area (Fig. 10a-c; western side of cross section). The opposite was true for the DRY simulations (Fig. 10d-f).

3.1.6. Near-surface air temperature

Supplementary Figure 1a-b shows diurnal changes in area average temperature and equivalent temperature for various land uses and different levels of irrigation applications. Changes to the surface energy balance are mainly responsible for the changes in near-surface air temperatures. When changes to the surface energy balance favor increased latent heat flux over sensible heat flux, near-surface air temperatures decrease, as found with the WET experiments (Supplementary Figure 1a). The opposite is true for the DRY experiments, where near-surface air temperatures increase due to higher sensible heat flux compared to latent heat flux. For WET experiments temperatures at 1500 UTC are approximately 1 °C lower compared to DRY experiments. It also needs to be noted that the 1500 UTC is local mid-morning and the temperature differences between the WET and DRY experiments are several orders of magnitude lower compared to the afternoon. Compared to CTRL, area average 2 m air temperatures decrease by 0.3, 0.4, and 0.4 °C for the WET05, WET10, and WET15 simulations, respectively (Table 5). On the other hand, area average 2 m air temperatures increase by 0.6, 0.4, and 0.4 °C for the DRY05, DRY10, and DRY15 simulations, respectively (Table 5).

Maximum air temperatures for the WET experiments are at 32.5, 32.4, and 32.2 °C (0.2, 0.3, and 0.5 °C decrease compared to CTRL) for the WET05, WET10, and WET15 simulations, respectively (Table 5). Maximum air temperatures for the DRY experiments are at 34.5, 34.8, and 34.8 °C (1.8, 2.1, and 2.1 °C increase compared to CTRL) for the DRY05, DRY10, and DRY15 simulations, respectively. These differences are due to different energy partitioning, where over the irrigated land cover, latent heat flux and over non-irrigated land use, sensible heat flux dominates. Thus, the added moisture introduced by irrigation reduced maximum near-surface air temperatures.

3.1.7. Near-surface equivalent temperature

Equivalent temperature (T_E) provides a complete account for total heat content (dry and moist) (Pielke et al., 2004; Matthews et al., 2022). This measure captures the contribution of moisture well (Fall et al., 2010; Schoof et al., 2014; Younger et al., 2019; Na-Yemeh et al., 2020). Moister air has higher T_E compared to air temperature and hence reflects the influence of irrigation on heat content of the atmosphere (e.g., Zhang et al., 2019). In this study, it is found that T_E responded to soil moisture changes (Supplementary Figure 1b and 2a-f). The WET experiments show increases of ~3 °C at 1500 UTC in the vicinity of the precipitation (Supplementary Figure 2a-c). Equivalent temperatures steadily increased with increased irrigation and soil moisture. On the other hand, the DRY experiments showed decreases of about 3 °C at 1500 UTC (Supplementary Figure 2d-f). The increased moisture content linked to irrigation is a contributing factor to the increased T_E. The area average T_E increased and decreased by 1 °C for the WET and DRY experiments, respectively (Table 5). Through early-mid-morning (1400 UTC), T_E could be higher over non-irrigated areas and subsequently becomes higher over the irrigated areas (Supplementary Figure 1b). Results also suggest that T_E is ~30 °C higher compared to near-surface air temperature which is consistent with previous findings linked to moist environments and irrigated land use (Younger et al., 2019; Zhang et al., 2019).

3.2. Non-irrigated area

Precipitation largely occurred over the irrigated region and since detailed discussions on precipitation is provided in the previous sections, additional assessment is not provided here. To represent realistic conditions, soil moisture was not changed over non-irrigated grid points and hence results are from the CTRL simulation over non-irrigated area (red box in Fig. 1). For brevity and to overcome redundancy, several subsections are combined below.

3.2.1. Latent and sensible heat flux

In the morning, smaller differences (~50 W m^{-2} at 1500 UTC) in latent heat flux are found between the irrigated and non-irrigated areas, but these differences are far greater (~260 W m^{-2}) in the afternoon hours (Fig. 9a). Latent heat flux is higher in the western portion of the study area for the rest of the analysis period. An exception is the evening hours where heat fluxes are at a minimum for both the irrigated and non-irrigated areas. Area average latent heat flux over the non-irrigated and irrigated areas are 56 W m^{-2} and 88 W m^{-2} (32 W m^{-2} difference), respectively (Table 5).

Sensible heat flux is higher over non-irrigated cropland in the morning and early afternoon hours, with the highest difference (77 W m^{-2}) at 1800 UTC (Fig. 9b). Average sensible heat flux over the irrigated and non-irrigated areas are 66 and 99 W m^{-2} (a 33 W m^{-2} difference), respectively (Table 5).

3.2.2. Planetary boundary layer height and vertical distribution of equivalent potential temperature

The non-irrigated and irrigated land use estimate PBLH of 753 m and 322 m (a 430 m difference), respectively at 1500 UTC. The highest difference (540 m) in PBLH between irrigated and non-irrigated areas is at 1700 UTC (Fig. 9c). It is found that area average PBLH over non-irrigated land and irrigated land uses are 634 m and 535 m, respectively (Table 5). In other words, PBLH is 99 m higher over non-irrigated land use. A cross-section of θ_e along with vertical wind vectors at 1500 UTC suggest descending motion and diverging winds in the areas of falling precipitation (Supplementary Figure 3). It is also evident that there was a pool of air with higher and lower θ_e above the irrigated and

non-irrigated area, respectively.

3.2.3. Near-surface air and equivalent temperature

The near-surface air temperatures over non-irrigated cropland are higher than over irrigated. Mean 2 m air temperatures over non-irrigated land use is 25.2 °C while it is 22.4 °C for irrigated land use (a 2.8 °C difference), at 1500 UTC. Maximum near-surface air temperatures over non-irrigated and irrigated land uses are 33.8 °C and 32.7 °C (a 1.1 °C difference), respectively (Table 5). Equivalent temperatures were rising over irrigated areas during the time of occurrence of precipitation. Subsequently, two maxima of differences (~2 °C) between irrigated and non-irrigated areas are found at 1800 UTC (~local midday) and 0000 UTC (Supplementary Figure 1b).

3.3. Grassland

3.3.1. Precipitation

Here we discuss the impacts of replacement of irrigated land use with grassland, approximating conditions prior to modern agriculture driven LULCC. Impacts of land use changes to grassland were investigated in several modeling studies in the past (Mahmood et al. 2011, Winchester et al. 2017, Rodgers et al. 2018). Unlike these modeling studies, where the dominant land use types were forests and grassland, the dominant land use types in this study, which is focused on Nebraska, are irrigated and non-irrigated agriculture. Thus, it would be of interest to analyze the impacts when irrigated land use is replaced by grassland.

Therefore, the irrigated grid points were replaced by grassland and no changes to soil moisture (i.e., CTRL soil moisture) were employed. Supplementary Figure 4a-d shows results from simulated reflectivity (precipitation), latent heat flux, sensible heat flux, and equivalent temperatures. The simulation found large increases (~3.5 times) in precipitation (149.37 mm; Fig. 5a smaller box) compared to CTRL (Table 4; Supplementary Figure 4a) at 1500 UTC. Area average precipitation over grassland increases to 3.2 mm compared to the 0.9 mm (a 2.3 mm difference) that fell across the irrigated region in CTRL. In other words, with grassland land use, there is a ~3.5 times area average increase in simulated precipitation compared to irrigated land use (Table 5). In addition, the GRASS simulation produced several fold increases in precipitation compared to all WET and DRY simulations (Tables 4 and 5). The general response of precipitation from the GRASS simulation is comparable to findings of Pielke et al. (1997).

3.3.2. Latent heat flux

Supplementary Figure 4b shows the GRASS – CTRL comparisons for latent heat flux at 1500 UTC. There are decreases in latent heat flux where the storms are present and increases before the storms initiated. At 1500 UTC, grasslands experience 4 W m^{-2} less hourly average latent heat flux than irrigated land use and ~12 W m^{-2} less than non-irrigated (Supplementary Figure 4b). Area average latent heat flux over grassland is 77 W m^{-2}, which is 11 W m^{-2} less than irrigated cropland (Table 5). Compared to the non-irrigated land use, latent heat flux is 21 W m^{-2} higher over grasslands. In comparison to the WET15 simulation, which estimates an average latent heat flux of 113 W m^{-2}, it was decreased by about one-third for grasslands. Compared to the DRY15 simulation, which has an average latent heat flux of 29 W m^{-2}, it is ~2.5 times higher over grasslands (Table 5).

3.3.3. Sensible heat flux

Sensible heat fluxes are higher before the precipitation cells enter the area and are lower while they are over the grassland area (Supplementary Figure 4c). The grassland area has a 6 W m^{-2} higher hourly average sensible heat flux compared to irrigated cropland at 1500 UTC. Compared to the non-irrigated cropland, hourly average sensible heat flux is 108 W m^{-2} lower over grassland at 1500 UTC (Table 5). Moreover, compared to irrigated cropland, the highest difference is found at 1700 UTC, when the grassland has a 92 W m^{-2} lower sensible heat flux.

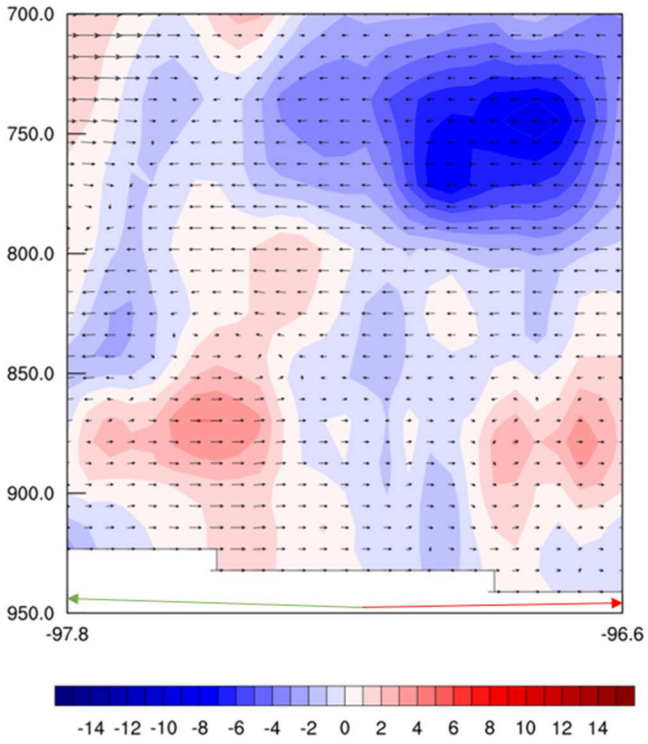

Fig. 11. GRASS - CTRL comparison of equivalent potential temperature (K) cross section (40.94° N Latitude) at 1500 UTC, 23 July 2018. Arrows delineate irrigated (green arrow) and non-irrigated (red arrow) land.

However, in the afternoon (2100 UTC) this is changed when grassland has a 30 W m^{-2} higher hourly average sensible heat flux compared to irrigated land use. It is found that the area average sensible heat flux over grassland is 67 W m^{-2} (1 W m^{-2} higher than over irrigated cropland) (Table 5). Compared to non-irrigated cropland, grassland has a 32 W m^{-2} lower area average sensible heat flux.

3.3.4. Planetary boundary layer height and vertical distribution of equivalent potential temperature

The PBLH is shallower and lower over grassland compared to irrigated cropland in the late morning and early afternoon hours (Fig. 9c). At 1500 UTC, hourly average PBLH was 81 m higher over grassland than over irrigated cropland while 349 m shallower over non-irrigated land use. The highest difference is found at 1900 UTC, when PBLH over grassland is 373 m shallower than for irrigated cropland (Fig. 9c). The PBLH is 832 m shallower at 1700 UTC over grassland compared to over non-irrigated land use. Area average PLBH over grassland is 517 m, which is 18 and 117 m shallower than irrigated and non-irrigated cropland, respectively (Table 5). In addition, compared to the WET15 simulation, area average PBLH over grassland is 48 m deeper while it is 136 m shallower compared to DRY15 (Table 5).

The GRASS simulation shows lower θ_e around 750 mb over grassland (west side of the cross section), but there was air with much lower θ_e over non-irrigated land use (east side of the cross section) at 1500 UTC (Fig. 11). Between the surface and 850 mb, higher θ_e dominates over grassland and implies a conducive environment for convection development.

3.3.5. Near-surface air and equivalent temperature

Hourly average near-surface air temperature is 0.3 (2.5) °C higher (lower) over grassland than over irrigated (non-irrigated) cropland at 1500 UTC (Supplementary Figure 1a). Compared to irrigated areas, near-surface air temperature remained lower over grassland after 1500 UTC, with differences reaching up to 1.4 °C at 1800 UTC. In the evening

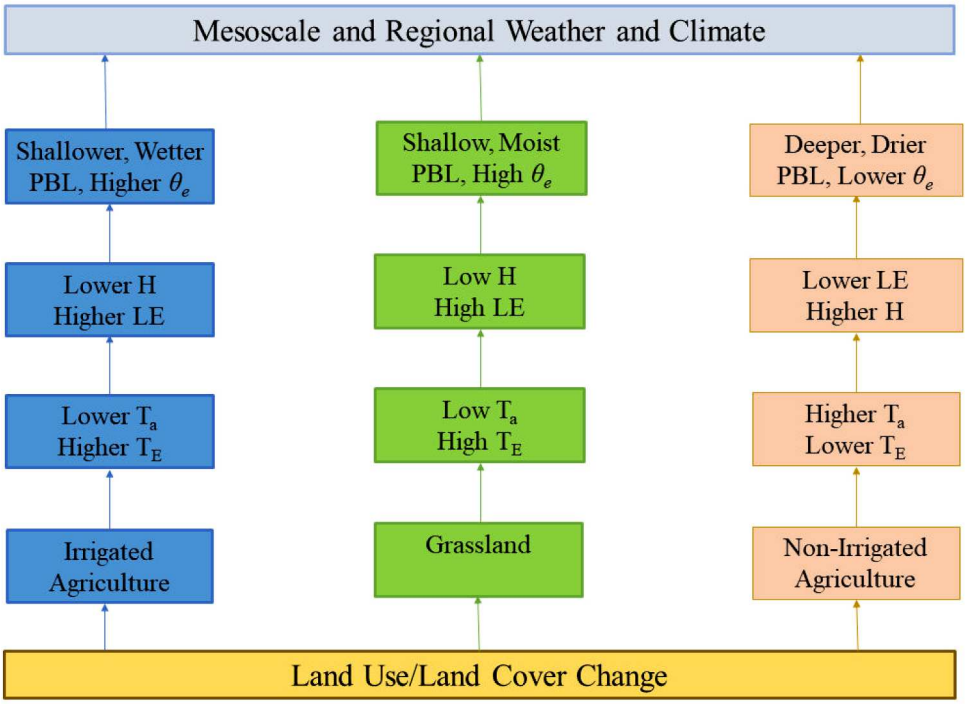

Fig. 12. A conceptual expression of LULCC and its impact on weather and climate. (Modified from Lachenmeier, 2020).

hours, grasslands are warmer by 0.9 °C around 0200 UTC on 24 July 2018. Maximum near-surface air temperature over grassland is nearly the same as irrigated land use and 1.1 °C lower over non-irrigated cropland (Table 5). Compared to WET15 and DRY15, maximum near-surface air temperature is 0.5 °C and 2.1 °C higher and lower over grassland, respectively. This is expected since sensible heat flux over grassland is lower than over non-irrigated and higher than over irrigated croplands.

Hourly area average T_E was rising before precipitation occurred (Supplementary Figure 1b). It was lower during and shortly after the precipitation, compared to over irrigated land use (Supplementary Figure 1b and 4d). Near precipitation, grassland T_E at 1500 UTC is ~2 °C lower compared to the irrigated and ~1 °C higher compared to the non-irrigated land uses (Supplementary Figure 4d). Analogous to irrigated and non-irrigated land use, T_E over grassland varies throughout the day and is higher and lower at times compared to irrigated and non-irrigated uses (Supplementary Figure 1b).

3.4. Summary

The model simulations demonstrate that changes in irrigation impact precipitation, surface energy balance, and the planetary boundary layer. Increases in irrigation increase (decrease) latent (sensible) heat flux and suggests that when the surface energy balance is dominated by latent (sensible) heat flux, the PLBH is shallower (deeper). For the event, initially increased irrigation resulted in lowering of precipitation and subsequently it increased. However, overall, precipitation declined with increased irrigation. On the other hand, decreases in irrigation initially dramatically increase precipitation but subsequently it declined rapidly with further decrease in irrigation and soil moisture. It is found that convection is enhanced (limited) where θ_e was higher (lower).

The grassland simulation demonstrates changes to the surface energy balance, the planetary boundary layer, and precipitation. The simulated reflectivity depicts a more organized convective system, delivering higher precipitation than when irrigation is present. The grassland simulation estimates less sensible heat flux than non-irrigated agriculture but more than irrigated agriculture. A shallower PBL is estimated over the grassland area compared to that over the irrigated and non-irrigated regions. Higher T_E are found at the surface over grassland. We suggest that the presence of grassland created an environment where latent and sensible heat flux were sufficiently high, allowing for the development of enhanced convection. The precipitation that occurred over grassland appeared to replenish soil moisture and subsequently increase latent heat flux and lower the PBLH during the afternoon.

The simulations showed a tendency to overestimate sensible heat flux which could result in unstable boundary layer and it is more noticeable for non-irrigated simulations. This also applies for irrigated land use simulations; however, sensible heat flux estimations are lower. On the other hand, latent heat flux estimations tend to be lower than observed. These under estimations are greater over non-irrigated areas. Overall, we suggest that the simulated precipitation over irrigated areas was satisfactory (as shown in Fig. 5a). Nonetheless, these biases should not be overlooked and be taken into consideration during interpretation of results here and elsewhere.

4. Conclusions

The rapid expansion of agriculture in the Great Plains during the 20th century, and the subsequent introduction of large-scale irrigation in Nebraska after 1945, is a notable example of LULCC. Although L-A interactions over various land use types have received attention, the understanding of these interactions for irrigated (and non-irrigated) agriculture can be further improved. To address this issue, the GRAINEX field campaign was conducted during the growing season of 2018. Several precipitation events were observed during this field campaign. The precipitation event discussed here occurred on 23 July 2018.

The current study analyzed the impacts of irrigation, non-irrigated crop land, and grassland on this event by using the Weather Research and Forecasting (WRF) model. Precipitation started over irrigated land near the irrigated-non-irrigated transition zone and dissipated over the non-irrigated land use. The underlying land use land cover provided a unique opportunity to assess their potential impacts on the event. Note that the precipitation occurred during a period when irrigation was at its maximum, during the peak growing season and high crop water

demand. To assess the impacts of various levels of irrigation, soil moisture was systematically modified across the irrigated grid cells within the WRF simulations. Soil moisture was not changed over the non-irrigated grid cells. The grassland simulation was designed to represent pre-irrigated and pre-European settlement LULC of Nebraska, i.e., without irrigation. For this simulation irrigated areas have been replaced with grassland. Soil moisture was not modified for the grassland simulation.

This research found that with increasing irrigation, and hence increasing soil moisture, precipitation at 1500 UTC for the event of interest declined. For DRY experiments precipitation initially increases but then declines. In other words, different levels of irrigation impacts precipitation amount. Increase (decrease) in latent (sensible) heat flux is found with increased irrigation during the time of precipitation. Similar results are found for the entire 24 hr simulations for different levels of irrigation. For example, WET15 (DRY15) has an area average latent heat flux of 113 W m^{-2} (29 W m^{-2}) while CTRL estimated a value of 88 W m^{-2}. The WET15 (DRY15) simulation estimates an area average sensible heat flux of 48 W m^{-2} (111 W m^{-2}) while CTRL simulation has a value of 66 W m^{-2}.

The planetary boundary layer over irrigated areas is shallower than over non-irrigated land use during the time of precipitation and on average. For example, The WET15, DRY15, and CTRL simulations estimate area average PBLH of 469, 653, and 535 m, respectively. WET (DRY) simulations increase (decrease) T_E up to 3 (2) °C higher compared to CTRL at 1500 UTC. Maximum near-surface air temperatures are reduced (increased) for the WET (DRY) simulations. It is also notable that T_E is about 28–30 °C higher over irrigated areas compared to near-surface air temperature. This suggests higher atmospheric heat content over irrigated land use.

The GRASS simulation produces higher area average precipitation totals compared to all other simulations. The simulation found large increases in precipitation (149.4 mm) compared to CTRL at 1500 UTC. An area average precipitation of 3.2 mm is estimated, which is nearly a three and a half times increase in precipitation compared to CTRL. The GRASS simulation has slightly lower latent heat flux compared to CTRL and WET simulations but higher than most of the DRY simulations around the time of precipitation. Similar results are found for area average latent heat flux (77 W m^{-2}), which is, again, less than CTRL and WET experiments but higher than the DRY experiments. The GRASS simulation found an area average PBLH of 517 m, which is shallower compared to the CTRL and DRY simulations but deeper than the WET simulations. In short, conditions over the grassland area are such that they provided a sufficient balance of latent and sensible heat flux, which allows turbulence to develop aiding the vertical transfer of moisture and the subsequent development of convection and precipitation. Fig. 12 further summarizes the current conceptual understanding of L-A interactions under three land use categories, supported by the findings of this study.

Moreover, this analysis is comprised of a robust number of simulations on a single precipitation event that occurred during the GRAINEX field campaign, which complement and support previous and current research on the impacts of irrigation on the Nebraska and Great Plains weather and climate. However, since this is a case study of a single precipitation event, further work is necessary prior to proposing a theoretical framework for the impacts of irrigation on precipitation in the Great Plains. From this study, it is also evident that the relationship between irrigation and precipitation can be non-linear and complex. Thus, in the future, additional research needs to be completed to further understand irrigation's impacts on precipitation. This research may include analysis of radar and radiosonde data and supporting modeling work.

Declaration of Competing Interest

The authors declare that they have no known competing financial interests or personal relationships that could have appeared to influence the work reported in this paper.

Data availability

Data will be made available on request.

Acknowledgements

The authors would like to thank two anonymous reviewers for their valuable comments and suggestions which helped to improve this manuscript. This research is funded by the National Science Foundation (NSF) grants AGS-1853390 (Rezaul Mahmood and Eric Rappin), AGS-1720477 (Udaysankar Nair), and AGS-1552487 (Roger Pielke Sr.). Mention of trade names or commercial products in this publication is solely for the purpose of providing specific information and does not imply recommendation or endorsement by the U.S. Department of Agriculture. USDA is an equal opportunity provider and employer.

Supplementary materials

Supplementary material associated with this article can be found, in the online version, at doi:10.1016/j.agrformet.2023.109854.

References

Barnston, A.G., Schikedanz, P.T., 1984. The effect of irrigation on warm season precipitation in the Southern Great Plains. J Clim. Appl. Meteor. 23, 865–888.
Chen, F., Dudhia, J., 2001. Coupling an advanced land surface-hydrology model with the Penn State-NCAR MM5 modeling system. Part 1: model implementation and sensitivity. Mon. Wea. Rev. 129, 569–585.
Chen, F., Warner, T.T., Manning, K., 2001. Sensitivity of orographic moist convection tolandscape variability: a study of the Buffalo Creek, Colorado, flash flood case of 1996. J. Atm. Sci. 58, 3204–3223.
Cook, B.I., Puma, M.J., Krakauer, N.Y., 2011. Irrigation induced surface cooling in the context of modern and increased greenhouse gas forcing. Clim. Dyn. 37, 1587–1600.
DeAngelis, A., Dominguez, F., Fan, Y., Robock, M., Kustu, M.D., Robinson, D., 2010. Evidence of enhanced precipitation due to irrigation over the Great Plains of the United States. J. Geophys. Res. 115. https://doi.org/10.1029/2010JD013892. D15115.
Dudhia, J., 1989. Numerical study of convection observed during the Winter Monsoon experiment using a mesoscale two–dimensional model. J. Atmos. Sci. 46, 3077–3107.
Earth Observing Laboratory, 2020. GRAINEX: the Great Plains irrigation experiment. Accessed 17 November 2020. https://www.eol.ucar.edu/field_projects/grainex.
Eltahir, E.A.B., 1998. A soil moisture–rainfall feedback mechanism. 1. Theory and observations. Water Resour. Res. 34, 765–776.
Evett, S.R., Colaizzi, P.D., Lamm, F.R., O'Shaughnessy, S.A., Heeren, D.M., Trout, T.J., Kranz, W.L., Lin, X, 2020. Past, present, and future of irrigation on the U. S. Great Plains. Trans. ASABE 63, 703–729.
Fall, S., Difenbaugh, N.S., Niyogi, D., Pielke Sr., R.A., Rochon, G., 2010. Temperature and equivalent temperature over the United States (1979–2005). Int. J. Climatol. 30, 2045–2054.
Holt, T.R., Niyogi, D., Chen, F., Manning, K., LeMone, M.A., Qureshi, A., 2006. Effect of land–atmosphere interactions on the IHOP 24–25 May 2002 convection case. Mon. Wea. Rev. 134, 113–133.
Hong, Song–You, Noh, Yign, Dudhia, Jimy, 2006. A new vertical diffusion package with an explicit treatment of entrainment processes. Mon. Wea. Rev. 134, 2318–2341.
Hong, S.–Y., Lim, J.–O.J., 2006. The WRF single–moment 6–class microphysics scheme (WSM6). J. Korean Meteor. Soc. 42, 129–151.
Huber, D.B., Mechem, D.B., Brunsell, N.A., 2014. The effects of Great Plains irrigation on the surface energy balance, regional circulation, and precipitation. Clim 2, 103–128.
Janjic, Z.I., 1994. The Step–Mountain Eta Coordinate Model: further developments of the convection, viscous sublayer, and turbulence closure schemes. Mon. Wea. Rev. 122, 927–945.
Kang, S., Eltahir, E.A.B., 2019. Impact of irrigation on regional climate over eastern China. Geophys. Res. Lett. 46, 5499–5505.
Kain, John S., 2004. The Kain–Fritsch convective parameterization: an update. J. Appl. Meteor. 43, 170–181.
Kueppers, L.M., Snyder, M.A., 2012. Influence of irrigated agriculture on diurnal surface energy and water fluxes, surface climate, and atmospheric circulation in California. Clim. Dyn. 38, 1017–1029.
Kustas, W.P., Hatfield, J.L., Prueger, J.H., 2005. The Soil Moisture–Atmosphere Coupling Experiment (SMACEX): background, hydrometeorological conditions, and preliminary findings. J. Hydrometeor. 6, 791–804.
Lachenmeier, E, 2020. Impacts of Irrigated Agriculture on the Near Surface and Planetary Boundary Layer Atmosphere: Results from the Great Plains Irrigation

Experiment (GRAINEX). M. S. Thesis. University of Nebraska-Lincoln, Lincoln, Nebraska, USA.
Lei, M., Niyogi, D., Kishtawal, C., Pielke Sr., R.A., Beltrán-Przekurat, A., Nobis, T.E., Vaidya, S.S., 2008. Effect of explicit urban land surface representation on the simulation of the 26 July 2005 heavy rain event over Mumbai, India. Atm. Chem. Phys. 8, 5975–5995.
Lawston, P.M., Santanello Jr., J.A., Hanson, B., Arsensault, K, 2020. Impacts of irrigation on summertime temperatures in the Pacific Northwest. Earth Inter. 24, 1–26.
Leeper, R., Mahmood, R., Quintanar, A., 2011. Influence of karst landscape on planetary boundary layer atmosphere: a Weather Research and Forecasting (WRF) model-based investigation. J. Hydrometeor. 12, 1512–1529.
Legates, D.R., McCabe, G.J., 1999. Evaluating the use of "goodness-of-fit" measures in hydrologic and hydroclimatic model validation. Water Resour. Res. 35, 233–241.
Lobell, D.B., Bonfils, C., 2008. The effect of irrigation on regional temperatures: a spatial and temporal analysis of trends in California. J. Clim. 21, 2064–2071.
Mahmood, R., Foster, S.A., Keeling, T., Hubbard, K.G., Carlson, C., Leeper, R., 2006. Impacts of irrigation on 20th-century temperatures in the Northern Great Plains. Glob. Planet. Change 54, 1–18.
Mahmood, R., Hubbard, K.G., 2002. Anthropogenic land use change in the North American Tall Grass-Short grass transition and modification of near surface hydrologic cycle. Clim. Res. 21, 83–90.
Mahmood, R., Hubbard, K.G., Carlson, C., 2004. Modification of growing season surface temperature records in the Northern Great Plains due to land use transformation: verification of modeling results and implication for global climate change. Int. J. Climatol. 24, 311–327.
Mahmood, R., Keeling, T., Foster, S.A., Hubbard, K.G., 2013. Did irrigation impact 20th century temperature in the High Plains Aquifer Region? Appl. Geogr. 38, 11–21.
Mahmood, R., Leeper, R., Quintanar, A.I., 2011. Sensitivity of planetary boundary layer atmosphere to historical and future land use/land cover, vegetation fraction, and soil moisture in Western Kentucky, USA. Glob. Planet. Change 78, 36–53.
Mahmood, R., Pielke, R.A., Hubbard, K.G., Niyogi, D., Dirmeyer, P.A., McAlpine, C., Carleton, A.M., Hale, R., Gameda, S., Beltrán-Przekurat, A., Baker, B., McNider, R., Legates, D.R., Shepherd, M., Du, J., Blanken, P.D., Frauenfeld, O.W., Nair, U.S., Fall, S., 2014. Land cover changes and their biogeophysical effects on climate. Inter. J. Climatol. 34, 929–953.
Mahmood, R., Schargorodski, M., Rappin, E., Griffin, M., Collins, P., Knupp, K., Quilligan, A., Wade, R., Cary, K., Foster, S., 2020. The total solar eclipse of 2017: meteorological observations from a statewide mesonet and atmospheric profiling systems. Bull. Am. Meteor. Soc. 101, E720–E737.
Matthews, T., Byrne, M., Horton, R., Murphy, C., Pielke, R.Sr, Raymond, C., Thorne, P., Wilby, R.L, 2022. Latent heat must be visible in climate communications. WIREs Clim. Change e779.
Mesinger, F., 1993. Forecasting upper tropospheric turbulence within the framework of the Mellor-Yamada 2.5 closure. In: Res. Activ. in Atmos. and Ocean. Mod., WMO, Geneva, CAS/JSC WGNE Rep. No. 18, 4.28-4.29.
Mesinger, F., DiMego, G., Kalnay, E., Mitchell, K., Shafran, P., Ebisuzaki, W., Jovic, D., Woollen, J., Rogers, E., Berbery, E., Ek, M., Fan, Y., Grumbine, R., Higgins, W., Li, H., Lin, Y., Manikin, G., Parrish, D., Shi, W., 2006. North American Regional Reanalysis. Bull. Amer. Meteor. Soc. 87, 343–360. Accessed in October 2020. https://rda.ucar.edu/datasets/ds608.0/.
Mlawer, Eli.J., Taubman, S.J., Brown, P.D., Iacono, M.J., Clough, S.A., 1997. Radiative transfer for inhomogeneous atmospheres: RRTM, a validated correlated–k model for the longwave. J. Geophys. Res. 102, 16663–16682.
Nair, U.S., Mark, H.R., Pielke Sr., R.A., 1997. Numerical simulation of the 9–10 June 1972 Black Hills storm using CSU RAMS. Mon. Wea. Rev. 125, 1753–1766.
Nair, U.S., Rappin, E., Foshee, E., Smith, W., Pielke Sr., R.A., Mahmood, R., Case, J.L., Blankenship, C.B., Shepherd, M., Santanello, J.A., Niyogi, D.A, 2019. Influence of land cover and soil moisture based brown ocean effect on an extreme rainfall event from a Louisiana Gulf Coast tropical System. Sci. Rep. 9, 17136.
Nauert, C.J., Ancell, B.C., 2019. Quantifying the effect of irrigation on nonlocal aspects of the atmosphere. J. Geophys. Res. 124, 7852–7867.
Na-Yemeh, D., Mahmood, R., Goodrich, G., Younger, K., Cary, K., Durkee, J., 2020. Growing season air mass equivalent temperature (TE) in the east central USA. Clim 8, 95, 1-17.
Nikiel, C.A., Eltahir, E.A.B., 2019. Summer climate change in the Midwest and Great Plains due to agriculture during the twentieth century. J. Clim. 32, 5583–5599.
Niyogi, D., Holt, T., Zhong, S., Pyle, P.C., Basara, J., 2006. Urban and land surface effectson the 30 July 2003 mesoscale convective system event observed in the southern Great Plains. J. Geophys. Res. 111, D19107. https://doi.org/10.1029/2005JD006746.
Ozdogan, M., Gutman, G., 2008. A new methodology to map irrigated areas using multi-temporal MODIS and ancillary data: an application example in the continental US. Remote Sens. Environ. 112, 3520–3537. https://sage.nelson.wisc.edu/data-and-models/datasets/. Accessed on October 2020.
Ozdogan, M., Rodell, M., Beaudoing, H.K., Toll, D.L., 2010. Simulating the effects of irrigation over the United States in a land surface model based on satellite-derived agricultural data. J. Hydrometeor. 11, 171–184.
Pielke Sr., R.A., 2001. Influence of the spatial distribution of vegetation and soils on the prediction of cumulus convective rainfall. Rev. Geophys. 39, 151–177.
Pielke Sr., R.A., Davey, C.A., Morgan, J., 2004. Assessing "global warming" with surface heat content. EOS Trans. 85, 210–211.
Pielke, R.A., Lee, T.J., Copeland, J.H., Eastman, J.L., Ziegler, C.L., Finley, C.A., 1997. Use of USGS-provided data to improve weather and climate simulations. Ecol. Appl. 7, 3–21.
Pielke, R.A., Mahmood, R., McAlpine, C., 2016. Land's complex role in climate change. Phys. Today 69, 40–46.
Pielke, R., Pitman, A., Niyogi, D., Mahmood, R., McAlpine, Hossain, F., Goldewijk, K.K., Nair, U., Betts, R., Fall, S., Reichstein, M., Kabat, P., de Noblet, N., 2011. Land use/land cover changes and climate: modeling analysis and observational evidence. WIREs Clim. Change. 2, 828–850.
Quintanar, A., Mahmood, R., Loughrin, J., Lovanh, N.C., 2008. A coupled MM5-Noah land surface model-based assessment of sensitivity of planetary boundary layer variables to anomalous soil moisture conditions. Phys. Geogr. 29, 54–78.
Rappin, E.D., Mahmood, R., Nair, U.S., Pielke Sr., R.A., 2022. Land-atmosphere interactions during GRAINEX: planetary boundary layer evolution in the presence of irrigation. J. Hydrometeor. 23, 1401–1417.
Rappin, E., Mahmood, R., Nair, U., Pielke, R., Brown, W., Oncley, S., Wurman, J., Kosiba, K., Kaulfus, A., Philips, C., Lachemeier, E., Santanello, J., Kim, E., Lawston-Parker, P., 2021. The Great Plains Irrigation Experiment (GRAINEX). Bull. Am. Meteor. Soc. 102, ES1756–ES1785.
Rodgers, W., Mahmood, R., Leeper, R., Yan, J., 2018. Land cover change, surface mining, and their impacts on a heavy rain event in the Appalachia. Annals Am. Assoc. Geogr. 108, 1187–1209.
Salmon, J.M., Friedl, M.A., Frolking, S., Wisser, D., Douglas, E.M., 2015. Global rain-fed, irrigated, and paddy croplands: a new high resolution map derived from remote sensing, crop inventories and climate data. Inter. J. Appl. Earth Obs. Geoinfor. 38, 321–334.
Schmid, P.E., Niyogi, D., 2017. Modeling urban precipitation modification by spatially heterogeneous aerosols. J. Appl. Meteor. Clim. 56, 2141–2153.
Schoof, J.T., Heern, Z.A., Therrell, M.D., Jemo, J.W.F., 2014. Assessing trends in lower tropospheric heat content in the Central USA using equivalent temperature. Int. J. Climatol. 35, 2828–2836.
Sen Roy, S., Mahmood, R., Quintanar, A., Gonzalez, A., 2011. Impacts of irrigation on dry season precipitation in India. Theor. Appl. Clim. 104, 193–207.
Skamarock, W.C., Klemp, J.B., Dudhia, J., Gill, D.O., Liu, Z., Berner, J., Wang, W., Powers, J.G., Duda, M.G., Barker, D.M., Huang, X.-Y. 2019. A description of the Advanced Research WRF Model version 4. NCAR Tech. Note NCAR/TN-556+STR, 145 pp., https://doi.org/10.5065/1dfh-6p97.
Sorooshian, S., Li, J., Hsu, K.L., Gao, X., 2011. How significant is the impact of irrigation on the local hydroclimate in Californias Central Valley? Comparison of model results with ground and remote-sensing data. J. Geophys. Res. Atm. 116, 1–11.
Suarez, A., Mahmood, R., Quintanar, A.I., Beltran-Przekurat, A., Pielke Sr . , R.A., 2014. A comparison of the MM5 and the Regional Atmospheric Modeling System simulations for land-atmosphere interactions under varying soil moisture. Tellus A: Dyn. Meteor. Ocean. 66, 21486. https://doi.org/10.3402/tellusa.v66.21486.
Szilagyi, J., Franz, T.E., 2020. Anthropogenic hydrometeorological changes at a regional scale: observed irrigation–precipitation feedback (1979–2015) in Nebraska, USA. Sustain. Water Resour. Manag. 6 (1) https://doi.org/10.1007/s40899-020-00368-w.
Tao, Wei–Kuo, Simpson, J., McCumber, M, 1989. An ice–water saturation adjustment. Mon. Wea. Rev. 117, 231–235.
Tao, W.-K., Wu, D., Lang, S., Chern, J.-D., Peters-Lidard, C., Fridlind, A., Matsui, T., 2016. High-resolution NU-WRF simulations of a deep convective-precipitation system during MC3E: further improvements and comparisons between Goddard microphysics schemes and obser- vations. J. Geophys. Res. Atmos. 121, 1278–1305.
Taylor, C.M., Klein, C., Parker, D.J., Gerard, F., Semeena, V.S., Barton, E.J., Harris, B.L., 2022. Late-stage" deforestation enhances storm trends in coastal West Africa. Proc. Natl. Acad. Sci. USA 119 (No. 2), e2109285119.
Tewari, M., Chen, F., Wang, W., Dudhia, J., LeMone, M.A., Mitchell, K., Ek, M., Gayno, G., Wegiel, J., Cuenca, R.H. 2004. Implementation and verification of the unified NOAH land surface model in the WRF model. 20th Conference on Weather Analysis and Forecasting/16th Conference on Numerical Weather Prediction, pp. 11–15.
USDA-ERS, 2021. https://www.ers.usda.gov/topics/farm-practices-management/irrigation-water-use/. Accessed on 06 March 2022.
Weckwerth, T.M., Parsons, D.B., Koch, S.E., Moore, J.A., LeMone, M.A., Demoz, B.B., Flamant, C., Geerts, B., Wang, J., Feltz, W.F., 2004. An overview of the international H2O project (IHOP_2002) and some preliminary highlights. Bull. Am. Meteor. Soc. 85, 253–257.
Whitesel, D., 2022. Irrigation's Impact on a Precipitation Event During GRAINEX in Nebraska, USA. M. S. Thesis. University of Nebraska-Lincoln, Lincoln.
Winchester, J., Mahmood, R., Rodgers, W., Hossian, F., Rappin, E., Durkee, D., Chronis, T., 2017. A model-based assessment of potential impacts of man-made reservoirs on precipitation. Earth Inter. 21, 1–31. https://doi.org/10.1175/EI-D-16-0016.1.
Xu, Z., Mahmood, R., Yang, Z.-L., Fu, C., Su, H., 2015. Investigating diurnal and seasonal climatic response to land use and land cover change over monsoon Asia with the Community Earth System Model. J. Geophys. Res. 120, 1137–1152. https://doi.org/10.1002/2014JD022479.
Younger, K., Mahmood, R., Goodrich, G., Pielke Sr., R.A., Durkee, J., 2019. Mesoscale surface equivalent temperature (T_E) for East Central USA. Theor. Appl. Climatol. 136, 65–75.
Zhang, T., Mahmood, R., Lin, X., Pielke Sr., R.A., 2019. Irrigation impacts on minimum and maximum surface moist enthalpy in the Central Great Plains of the USA. Wea. Clim. Extrem. 23, 100197.